AN ABSTRACT OF THE THESIS OF

Yung-Chun Gao for the degree of Master of Science in Nuclear Engineering presented on December 11, 1981

Title: Neutron and Gamma Radiography of UO_2 Fuel and TRIGA Fuel Elements

Redacted for privacy

Abstract approved: A. H. Robinson

Neutron radiography is a very useful method for the nondestructive inspection of nuclear fuels. Such radiographs can be used to view the internal structure of individual fuel pins before (or after) placing them in a nuclear reactor. Neutron radiographs of uranium dioxide fuel (UO_2) have been used to detect defects in the fuel such as cracks, voids, position errors, dimensional errors, enrichment differences, end-capping, and a variety of other manufacturing defects.

The main purpose of this work was to develop a method of radiographing the TRIGA fuel elements used in the Oregon State University TRIGA Reactor (OSTR). These fuel elements are especially difficult to radiograph using neutron radiography techniques because of the high hydrogen content of these elements. The hydrogen in the TRIGA fuel causes a

large amount of scattering of the neutron beam used to obtain the radiographs. This scattering causes significant blurring of the image of the internal structure of the fuel. In this thesis a method of radiographing these elements is presented that provides excellent results. This method, which uses gamma radiation, allows the internal structure of TRIGA fuels to be viewed.

In order to develop this method, seven UO_2 fuel elements were constructed with known defects. These elements, which contain no hydrogen, could be radiographed with either neutron or gamma radiography. The results of this work showed that a neutron radiography facility could be used to produce excellent gamma radiographs. These gamma radiographs showed nearly all the defects visible in the neutron radiographs.

The gamma radiography technique developed for the special UO_2 fuel pins was then applied to the TRIGA fuel elements. The resulting radiographs revealed the internal structure of these elements. Four types of defects were detected in the TRIGA fuel elements. These were voids, cracks, broken zirconium parts, and fuel slugs that were sheared into two parts. Other details, such as the fuel to clad spacing, were also visible in these radiographs.

NEUTRON AND GAMMA RADIOGRAPHY OF UO_2 FUEL AND TRIGA FUEL ELEMENTS

by

Y. C. Gao

A THESIS

submitted to

Oregon State University

in partial fulfillment of
the requirements for the
degree of

Master of Science

Completed December 11,1981

Commencement June 1982

APPROVED:

Redacted for privacy

Professor of Nuclear Engineering
in Charge of Major

Redacted for privacy

Head of Department of Nuclear Engineering

Redacted for privacy

Dean of Graduate School

Date thesis is presented December 11, 1981

Typed by Y. C. Gao

ACKNOWLEDGEMENT

The work presented in this thesis has benefitted from the help of Dr.C.H.Wang, without his effort and encouragement this work would not have been possible.

I have to give my sicerest thanks to my major professor, Dr.A.H.Robinson, for his guidance, encouragement, and patience.

Also I would like to give my thanks to Dr.J.C.Ringle, Prof.A.J.Johnson, Dr.S.E.Binney, Dr.B.Dodd, T.Anderson, B.Carpenter, R.Keen, E.Flickinger for their help.

I would like to dedicate this work to my motherland, The People's Republic of China, for its love, and support.

TABLE OF CONTENTS

LIST OF FIGURES

LIST OF TABLES

NEUTRON AND GAMMA RADIOGRAPHY OF UO_2 AND TRIGA FUEL ELEMENTS

I. INTRODUCTION

1.1 Background

The use of X-ray radiography to look through objects which do not transmit light has been a more or less commonplace occurrence practically from the day Roentgen announced his discovery of X-rays more than a half-century ago. Neutron radiographic techniques originated from investigations by H. Kallmann and E. Kuhn (1) in Germany in 1935. Thewlis (2) renewed this work in the 1950's; however, significant application and development did not occur until the 1960's. Some authors (3,4) suggest that the reason for the thirty year delay between discovery and practical application of neutron radiography lay in the availability of a suitable neutron source, industrial knowledge of neutron radiography methods, and the development of standards for taking neutron radiographs. During the last two decades the expansion has indeed been rapid. A number of publications on the general principles and applications have been written (3-9). In addition, a large volume of material on special techniques for neutron radiography has been published. Today, neutron radiography

is routinely used for nondestructive examination of suitable objects with appropriate standard procedures. These procedures are certified in many countries in the world. In this country, standards have been developed by the American Society for Non-destructive Testing (ASNT) and the American Society for Testing Materials (ASTM) (4).

1.2 General Radiography

An ordinary photograph is taken by having light reflect off the object, thereby giving an image of the surface. Radiographs (X, gamma or neutron) are made by passing the appropriate type of radiation through the object and recording the image of the transmitted beam. Such radiographs reveal details about the materials inside the object.

The general radiographic process is shown in Figure 1.1. A uniform radiation beam passes through the object which spatially modulates the beam due to the different interaction coefficients of the elements comprising the object. The transmitted beam then impinges on the imaging system represented by the imaging plane in the figure. The basic differences among the types of radiography lie in: (a) the interaction between the radiation beam and the object; (b) the radiation source; and (c) the imaging techniques. The significance of neutron radiography is based on the fact that the attenuation of neutrons by materials differs entirely from the attenuation of X- and gamma rays. The attenuation of thermal neutrons in light and heavy materials is often the reverse of that of X- and gamma rays. This difference in attenuation leads to neutron radiographic discrimination of many elements which cannot be done with conventional X- and gamma radiography.

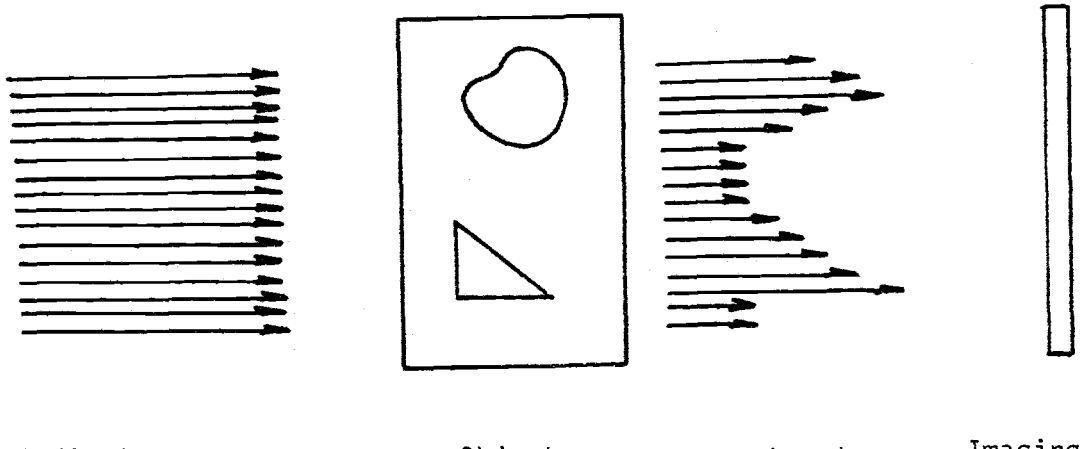

Fig.1.1. General Radiographic Process

X-rays are a form of electromagnetic radiation similar to gamma rays, visible light, and radio waves, but they differ in wavelength and quantum energy. When X or gamma rays pass through matter they usually interact with the orbital electrons of the atom. X- or gamma ray attenuation increases for higher atomic numbers because of increased electron cloud density. Neutrons, on the other hand, are not influenced by the electron cloud and interact only with the nuclear forces. Neutrons interact with nuclei in several ways; such as elastic scattering, inelastic scattering, and absorption. The probabilities of these events are represented by effective cross sections. Neutron cross sections vary with neutron energy, nuclear spin states, neutron/proton ratio, atomic number and several other nuclear and quantum mechanical phenomena. For a given energy of the incident neutron beam, and particularly for lower neutron energies, the microscopic neutron cross section varies abruptly between adjacent elements in the periodic table. Cross sections also change abruptly from one isotope to another for certain elements. The macroscopic cross section of a material can be calculated by adding the product of microscopic cross section for each type of interaction by the nuclei number density (atoms/barn-cm). In Figure 1.2 this number is divided by the material density and called the mass attenuation coefficient. This figure shows how the mass

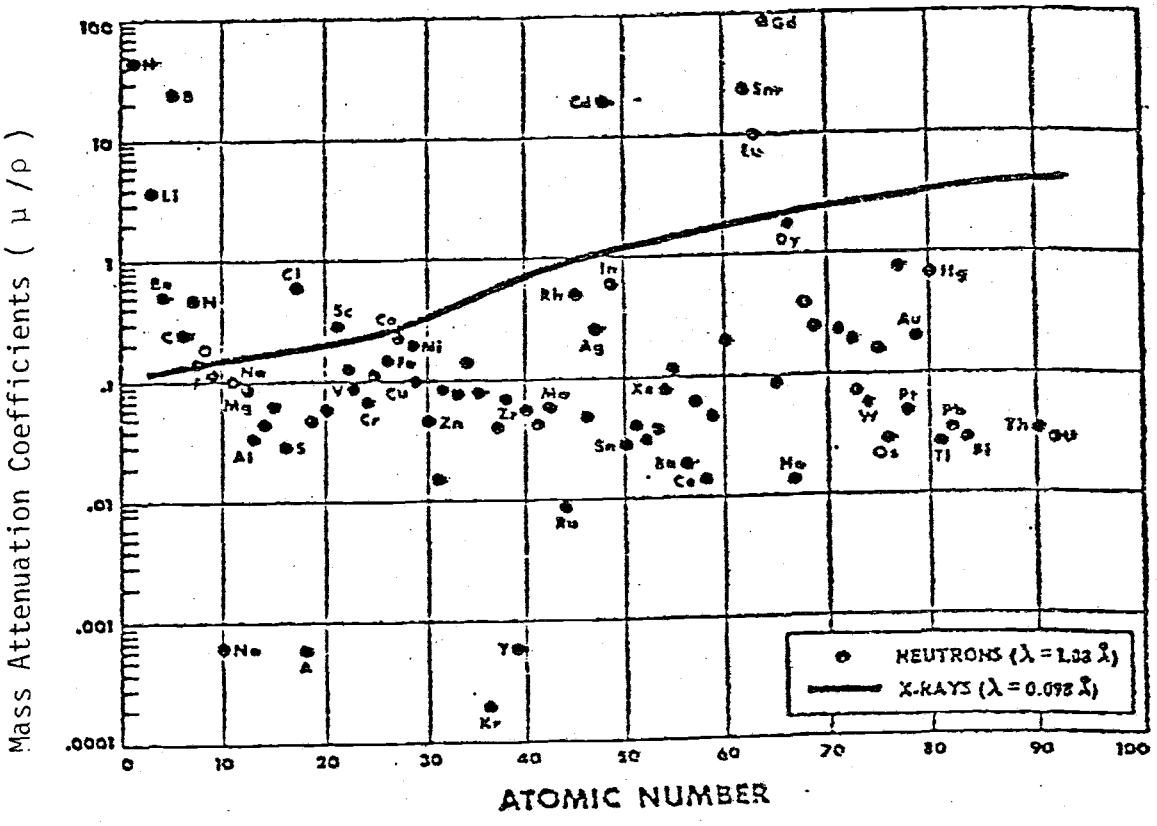

Fig.1.2 Mass Attenuation Coefficients versus Atomic Number for Both Thermal Neutrons and X-rays

attenuation coefficients for the thermal neutrons vary for different elements. This may be contrasted to the well known increase in X-ray attenuation coefficients with increasing atomic number. A high attenuation means high contrast for a small thickness of materials; low attenuation means that a large thickness can be more easily penetrated. For inspection purposes, this difference has made neutron, X- and gamma radiography complementary techniques.

In addition to the difference in the attenuation between neutrons and X-rays, the imaging technique also varies. Many types of direct exposure X-ray films are now available. At present, no direct exposure neutron films exist. This is due to the fact that neutrons do not interact significantly with photographic film media. Instead, film exposure is achieved by using converters or scintillator screens. These screens or converters are used to change neutron radiation into localized ionizing radiation or light. The actual technique will depend on the type of the neutron radiography (static, pulsed or high speed motion) being performed, and on the specific requirements for image quality and resolution.

As noted, there are three basic types of neutron radiography: static, pulsed, and high speed motion. For static neutron radiography, the source is at a constant strength, the object is stationary, and the imaging system

is a converter foil. For pulsed neutron radiography, the neutron source is a pulsed neutron generator or a nuclear reactor which has the capability of pulsing from a low neutron level to an extremely high one followed by a return to a low level all in a few milliseconds. The object is stationary or slowly moving, and the imaging system is a converter foil or other suitable imaging method. High speed neutron radiography uses a reactor with pulsing capability. The object can be stationary, slowly moving, quickly moving , or in continuous motion. The imaging system contains a scintillator screen, a light image intensifier and a high speed camera.

1.3 Basic Neutron Radiography Techniques

In static direct neutron radiography, a thin foil with a high neutron absorption cross section, such as gadolinium, is placed in a cassette with X-ray film and is then placed in the neutron beam. This arrangement is shown in Figure 1.3 (a). Neutrons absorbed in the gadolinium nuclei cause the emission of electromagnetic energy which generates internal conversion electrons in the gadolinium. These electrons then expose the film. This technique, using a very thin gadolinium foil or a vapor-deposited gadolinium layer and fine grain film, presently provides the highest quality neutron radiographs.

In the transfer method, as shown in Figure 1.3 (b), a converter foil is placed in the beam behind the object to be examined. The foil is subsequently activated (made radioactive) by the neutrons transmitted through the object. After irradiation, the foil is placed against a piece of film and allowed to decay for several half lives. The film detects beta and gamma emissions from the foil and records a pattern characteristic of the relative activation on the surface of the foil. Since no gamma radiation from the core or from a possibly radioactive object can contribute to the exposure of the film, this technique provides a radiograph that is free of any gamma image. This method permits examination of highly radioactive objects.

Fig. 1.3

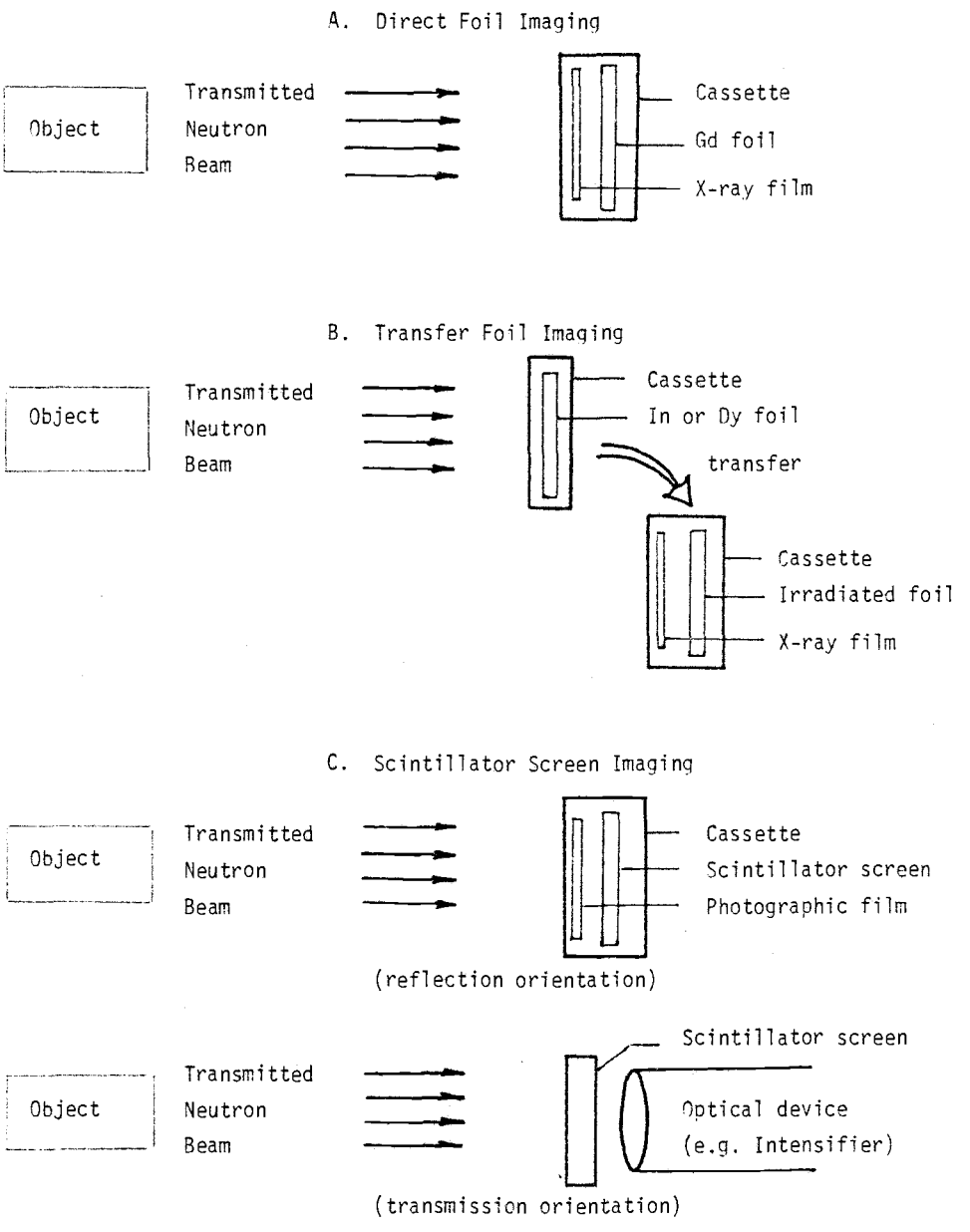
A. Direct Foil Imaging
Object
Transmitted
Neutron
Beam
Cassette
Gd foil
X-ray film
B. Transfer Foil Imaging
Object
Transmitted
Neutron
Beam
Cassette
In or Dy foil
transfer
Cassette
Irradiated foil
X-ray film
C. Scintillator Screen Imaging
Object
Transmitted
Neutron
Beam
Cassette
Scintillator screen
Photographic film
(reflection orientation)
Object
Transmitted
Neutron
Beam
Scintillator screen
Optical device
(e.g. Intensifier)
(transmission orientation)

Fairly high fluxes of neutrons (above 10^7 at the object) are desirable for the transfer method since the induced activity in a transfer screen saturates after a few half-lives and a longer exposure can not be used to compensate for low beam intensity. For the transfer method, medium half-life materials with a high thermal neutron cross section, such as europium, indium, or dysprosium, must be used.

Radiography with neutrons in the epithermal or resonance energy region, which is approximately 1.0 eV to 10 keV energy, has been concentrated mainly in the lower energy end of that spectrum. Although neutron cross sections tend to decrease as the neutron energy increases above the thermal energy range, there are also large resonances in cross section that occur in this energy region. Therefore, detectors such as indium with a large activation resonance at 1.46 eV have been used as a detector for these neutrons. Gold, with a resonance at 4.9 eV, and tungsten, with a resonance of 18.8 eV, are other potentially useful detectors. Epithermal radiography is normally performed with a cadmium sheet to filter the neutron beam. This removes thermal neutrons from the beam. Epithermal radiography may be performed using either the direct method or the transfer method.

In the neutron radiography of transient phenomenon, the time necessary to produce an image must be reduced.

Neutron intensities available from research reactors operating at their maximum steady power are not high enough to allow the speed required for such special applications of neutron radiography. In industrial neutron radiography, resolution is of prime importance and is obtained using long exposure times. The motion of some objects or the kinetic behavior of radio-opaque agents tends to blur the images. Neutron radiography using steady power reactors requires times ranging from 1 to 2 hours in extremely high resolution applications to seconds using some advanced but unfortunately low resolution imaging systems.

The solution to this problem is to obtain neutron radiographic images in time scale orders of magnitude shorter than previously possible. This can be accomplished by using a pulsing reactor. This type of reactor can produce extremely high neutron intensities for very short periods of time. With the Oregon State University TRIGA Reactor (OSTR), exposures equivalent to one minute of full power operation can be compressed into a 15 millisecond flash.

Using this pulsing capability, a high speed motion neutron radiography system has been constructed at Oregon State University. This system is capable of producing a neutron radiograph in 40 μseconds. The radiographs are recorded on movie film with frame rates up to 10,000 per second. The system makes use of neutron scintillators to

convert the neutron image to a light image. This light image is then amplified before being recorded on film.

Scintillator systems are very efficient and can produce a satisfactory, although somewhat grainy, radiographs. By using a scintillator converter system in conjunction with a light image intensifier and a high speed camera system, it is possible to study objects in rapid motion.

Scintillator screens contain a high neutron absorption cross section material such as ^{6}Li, ^{10}B or ^{155}Gd plus a scintillation material. Following neutron absorption, the scintillation material, such as zinc-sulphide, is stimulated by charged particles from the neutron interaction and light is emitted, as shown in Figure 1.3 (c). The light may be used to expose light sensitive film or as input into other optical devices. This technique requires the least exposure of any method for taking neutron radiographs and is the fastest detection method.

In a single radiograph all images are superimposed. This can cause some difficulty in interpreting the information in the radiograph. Stereoradiography is one method for seeing the relative positions of objects in the radiographs. In stereo X-radiography the technique involves shifting the X-ray tube a distance determined by the focus-film distance and the eye-radiograph viewing distance. The procedures for X-radiography are described

in references 10 and 11. For focus-film distance greater than 60 inches, a tube shift of 1:10 is generally used. Excellent neutron stereoscopic pictures can be obtained by the simple expedient of rotating the object between exposures while leaving the imaging system in the same position related to the reactor beam. A number of stereoscopic pairs of neutron radiographs were taken by Robinson and Porter (12) using this technique. The principle and the procedures for gamma stereo radiography are the same as that for neutron stereo radiography.

1.4 Review of Some Neutron Radiography Applications

The majority of the industrial applications for neutron radiography that have been developed to date use neutrons of thermal energy. This is because (a) thermal neutron beams are easy to obtain, (b) thermal neutrons can be detected effectively, and (c) there is a useful variety of contrasts for different materials. The predominate areas of neutron radiography application have been in the inspection of hydrogenous materials and heavy elements. Ordnance devices, consisting of a hydrocarbon encased in a metal container, are relatively insensitive to X- or gamma ray interrogation and hence require neutron radiography inspection (13). Nuclear fuel made of uranium or plutonium cannot be adequately inspected with X- or low energy gamma rays for other than gross surface flaws behind the cladding due to the limited penetration of the beam and lack of contrast. Neutron radiography provides an effective inspection method for fuel elements with the ability to show the enrichment, segregation and internal flaws both before and after use in a reactor (14-19). However, many details of fuel elements can also be seen using high energy gamma radiography. This is one of the main conclusions of this study.

Since X-rays interact with the electron cloud of the atom, different isotopes cannot be distinguished by X-

radiography. With neutron radiography, however, the different neutron interaction cross sections of the isotopes allow for significant image differentiation; such as with ^{235}U in ^{238}U. Another example is the ability to study the transformation of ^{113}Cd to ^{114}Cd by neutron capture after usage as a reactor control plate (20). This difference in capabilities is one of the major reasons for the continued development and increasing scope of applicability for neutron radiographic techniques. Some light elements which do not differ very much in atomic number, such as beryllium and boron, or boron and carbon, reveal considerable differences in neutron absorption. This indicates the possibility of radiographic discrimination between neighboring elements using neutron radiography. This is not feasible with X- or gamma rays, as the X- or gamma ray absorption coefficients for the elements mentioned above are very similar. Neutron radiography has also been applied in specific instances to the detection of hydriding in titanium and zirconium (21,17). For detection of hidden corrosion, neutron radiography appears to hold a distinct advantage over other techniques in its ability to image the corroded sites (22,23).

Although progress has not been rapid, medical and biological applications do exist for neutron radiography for which some successful work has been accomplished

(24-27). Supplementing these applications, there has been a continual development of special techniques, such as the use of very low energy, epithermal or fast neutrons in neutron radiography to gain increased contrast sensitivity or penetration in objects (28-33).

Non-reactor sources have been employed for economic reasons and transportability (34-37). New imaging methods have been developed such as electronic techniques and track-etching (38-40).

A tendency can be seen whereby industries are prepared to look beyond the capabilities of straightforward thermal neutron radiography. For certain special problems, development work is being undertaken to tailor techniques to meet particular needs. One example of this is the previously mentioned high-speed neutron radiography facility now in operation at Oregon State University. This facility is used to examine the actual firing process of propellents during the one millisecond or less that such a process may last (41). Another example is the development of highly-transportable neutron radiography equipment for inspection of aircraft (23).

1.5 Scope of this Study

The main purpose of this study was to develop a method for radiographing TRIGA fuel elements. Early in the work it became apparent that neutron radiography would not be satisfactory due to the hydrogen content of the fuel. For this reason, a method using high energy gamma rays was developed.

Radiography of UO_2 fuel was performed with both neutron and gamma radiography so that the ability of gamma radiography to see fuel defects could be evaluated. This work describes how to take high quality gamma radiographs of TRIGA fuel. Using this method, a number of fuel defects were detected which were not visible in neutron radiographs.

Any radiography facility must be carefully designed to meet the objectives of the program. The system design used in this work will be discussed in chapter II. One of the most important parts of the system is the neutron converter screens or scintillators used to record the image. Chapter II presents a discussion of these converter screens or scintillators and how they were used in this study.

All of the neutron and gamma radiographs for this study were taken at the OSTR. Chapter III describes the basic charateristics of this reactor and the beam port facilities used for neutron radiography.

Special UO_2 fuel pins and TRIGA fuel elements were radiographed by using both neutron and gamma radiography. The results will be presented in chapters IV and V, respectively.

II. RADIOGRAPHY SYSTEM DESIGN

2.1 Requirements for Radiography

The requirement for an X-ray source can be achieved by using either an X-ray machine or a radioactive isotope. For gamma radiography, the source can be an intense radioisotope source or a nuclear reactor. Similarly, for neutron radiography, the neutron source can be an accelerator which generates neutrons, a neutron emitting isotope such as californium-252, or fission neutrons from a nuclear reactor can fulfill the requirement for neutron radiography. The common radiographic isotope sources and some of the neutron producing reactions for accelerators and reactors are listed in Table 2.1.

At the present stage of neutron source development, the highest quality neutron radiographs produced have been made using nuclear reactors for neutron sources. The high thermal neutron beam intensities available from such sources account for this fact. Typical research reactors operate at a peak steady state flux level of 10^{12} to 10^{13} n/cm^2-sec. A few high flux reactors, such as the ATR at Idaho Falls and HFIR at Oak Ridge, have peak fluxes on the order of 10^{15} n/cm^2-sec.

A number of different types of reactors have been used for radiography, such as the graphite-moderated BEPO

TABLE 2.1 NEUTRON PRODUCING REACTIONS FOR RADIOISOTOPE SOURCES, ACCELERATORS, AND NUCLEAR REACTORS.

Radioisotope	Reaction
^{124}Sb-Be	(γ,n)
^{210}Po-Be	(α,n)
^{239}Pu-Be	(α,n)
^{241}Am-Be	(α,n)
^{242}Cm-Be	(α,n)
^{252}Cf	(sf)

Reactions for Accelerators

$^{2}H\ (d,n)\ ^{3}He$

$^{3}H\ (d,n)\ ^{4}He$

$^{9}Be(d,n)\ ^{10}B$

Reactions for Nuclear Reactors

$^{235}U\ (n,f)\ n$

reactor at Harwell, the heavy-water moderated reactor at Argonne National Laboratory, the light-water moderated Armour Research Reactor, the water boiler reactor at Los Alamos, the light-water cooled and moderated at Battelle Research Reactor, the Juggernaut reactor at Argonne National Laboratory, and the liquid metal cooled nuclear reactor at Hanford, Washington.

In typical light photography the light image from the object to be photographed can be focused onto the film using a lens. However, neutrons cannot be focused and collimation of the neutrons from the source is required in order to get a suitable beam for radiography. The problem is to produce a beam of neutrons in which the neutron directions are nearly parallel. At the OSTR this is accomplished by using a collimator in the beam port #1 facility. This collimator, which will be described in chapter III, makes the neutron source appear to be a nearly point source. Neutrons arriving at the object from a point source have nearly parallel directions.

Although the specific imaging method depends greatly on the type of neutron radiography being performed, the general requirements are as follows:

(a) a means of converting the transmitted spatially modulated neutron beam from the object/event into an ionizing radiation beam which can be recorded on some type of photographic film;

(b) an appropriate type of film for recording the image;

(c) the ability to control the exposure of the film.

The major film requirement for neutron radiography is that the film must be adequately sensitive to the type and amount of ionizing radiation produced by the converter foil or screen.

The shielding at a research facility for neutron or gamma radiography should be designed such that radiation exposure to personnel and equipment is minimized, and personnel are protected in a positive manner from accidental radiation exposure.

2.2 COLLIMATION

In this section the collimators for neutron radiography are described. However, the same collimation methods may be used for gamma radiography. At the OSTR the same facility can be used for both neutron and gamma radiography. For fast neutron radiography, an accelerator or radioactive isotope may be used as a point source in geometries similar to those used for X-radiography.

In typical thermal neutron radiography, the neutrons in the reactor are moving equally in all directions. In order to get a parallel beam a special collimator system must be used. The collimator for a radiography system serves to select the neutrons or gamma rays that are in a nearly parallel path by removing neutrons or gamma rays which are moving in the wrong direction.

The length to diameter ratio (L/D) of the collimator is the parameter used to measure the collimator quality. L is the distance that the neutrons travel from the collimator to the object and D is the smallest diameter opening in the collimator. The larger the L/D ratio is, the more parallel the neutron beam will be. The effect of the L/D ratio on the resolution capability of a system is shown in Figure 2.1. A larger L/D ratio, shown in Figure 2.1 (a), results in a smaller imaging area on the film. A small L/D ratio can result in a significant amount of blurring of the

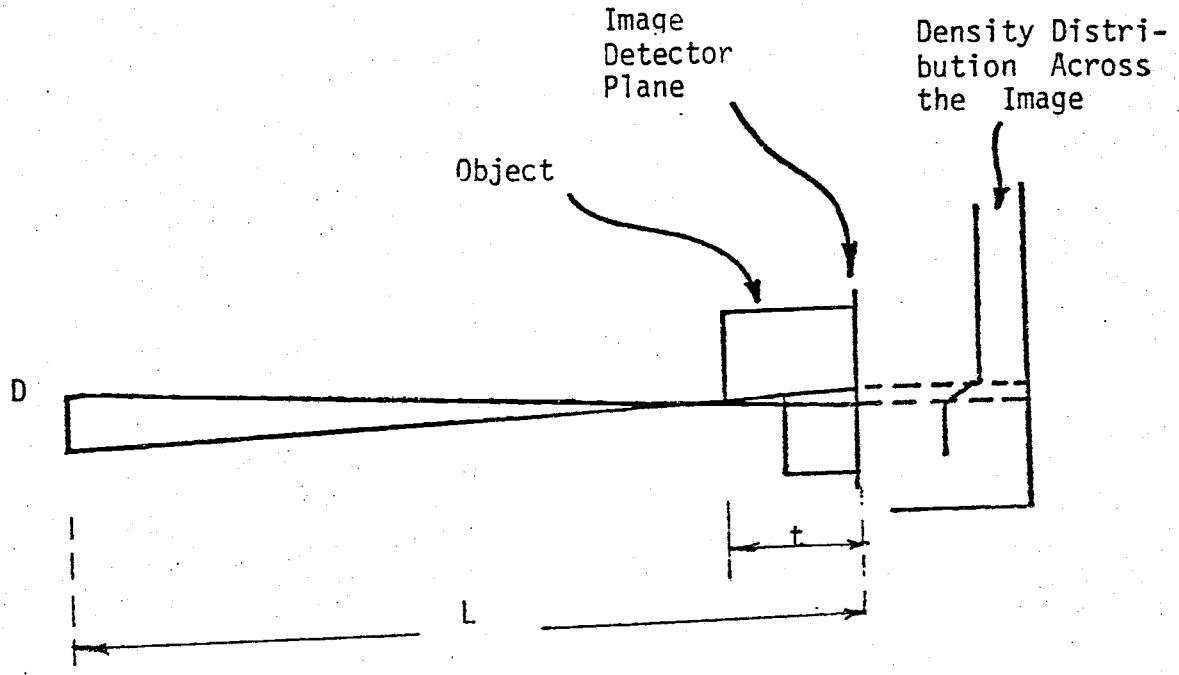

Fig.2.1 (a). Large L/D Resolution Effect.

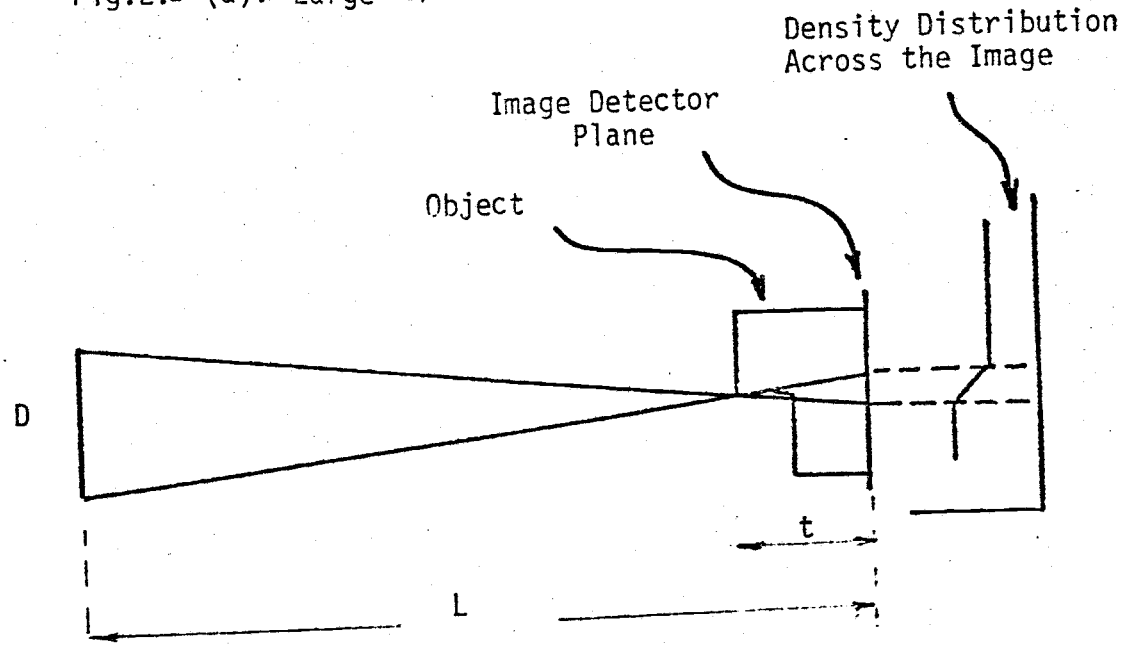

Fig.2.1 (b). Small L/D Resolution Effect.

imaging as shown in Figure 2.1 (b).

Collimators may be of several types, for example, solar slit, divergent and convergent-divergent (42-44), stepped divergent (45), as well as the pin-hole type used at OSU. Due to its simplicity, the pin-hole type is one of the most frequently chosen types in recently constructed facilities.

Beam port #1, used for stationary neutron or gamma radiography at the OSTR, has an L/D ratio which can be varied from about 600:1 to about 100:1, depending upon the desired resolution. The variable ratio is due to a variable aperature, which has a minimum diameter of 0.25 inches and 1.5 inches fully open.

2.3 Objects and Events

A good example of the type of object which is suitable for neutron radiography is shown in Figure 2.2. This figure shows a static neutron radiograph of a flashlight. This flashlight was also radiographed by X- and gamma rays, as shown in Figures 2.3 and 2.4. These pictures reveal some very important differences between neutron radiographs and X- or gamma radiographs. All the pictures are positive prints, and first show that X-, gamma and neutron radiographs give the same imaging of some parts of this flash light. For example, the batteries, light bulb, and metal part of the head of the flashlight can be seen in every picture. However, these pictures also show that neutron radiography is superior for this object in that it provides excellent overall visibility of the flashlight internal details. Specifically, the neutrons image the light density materials of the flashlight best, especially the plastic head cup. The imaging of the light bulb area, the magnetic holder, the switch part and the batteries of the flashlight on the neutron radiograph show much more detail and contrast than the other two radiographs. However, some metal parts of the flashlight, such as the spring, the metal tube, and the half cone connector show better detail in the X-radiograph than the neutron or gamma radiographs.

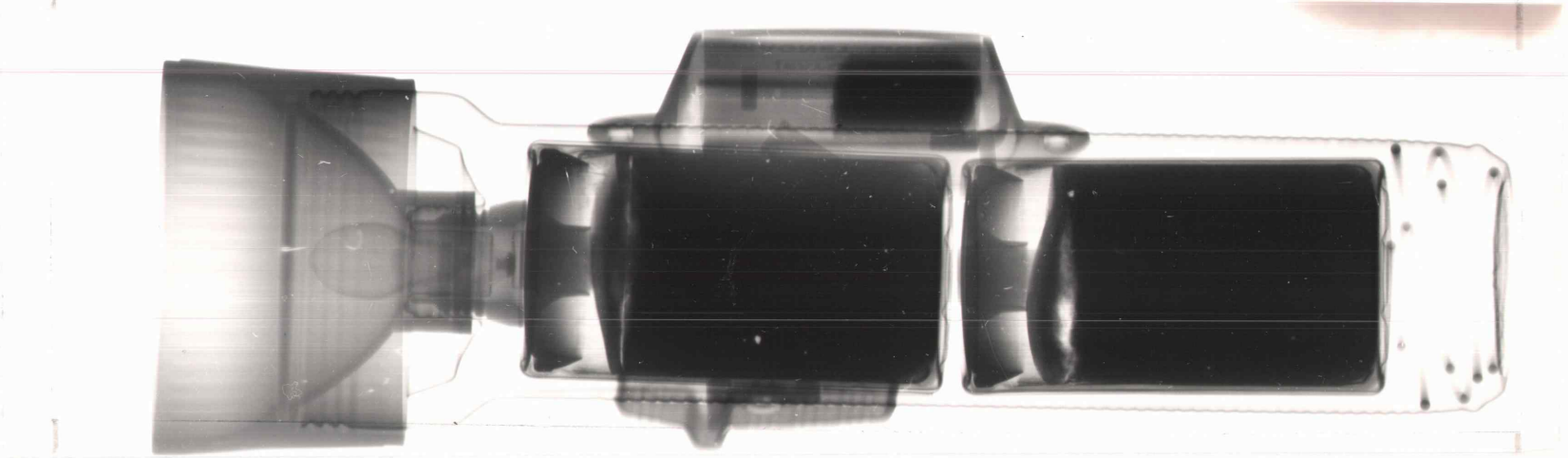

Figure 2.2 Neutron Radiograph of Flashlight

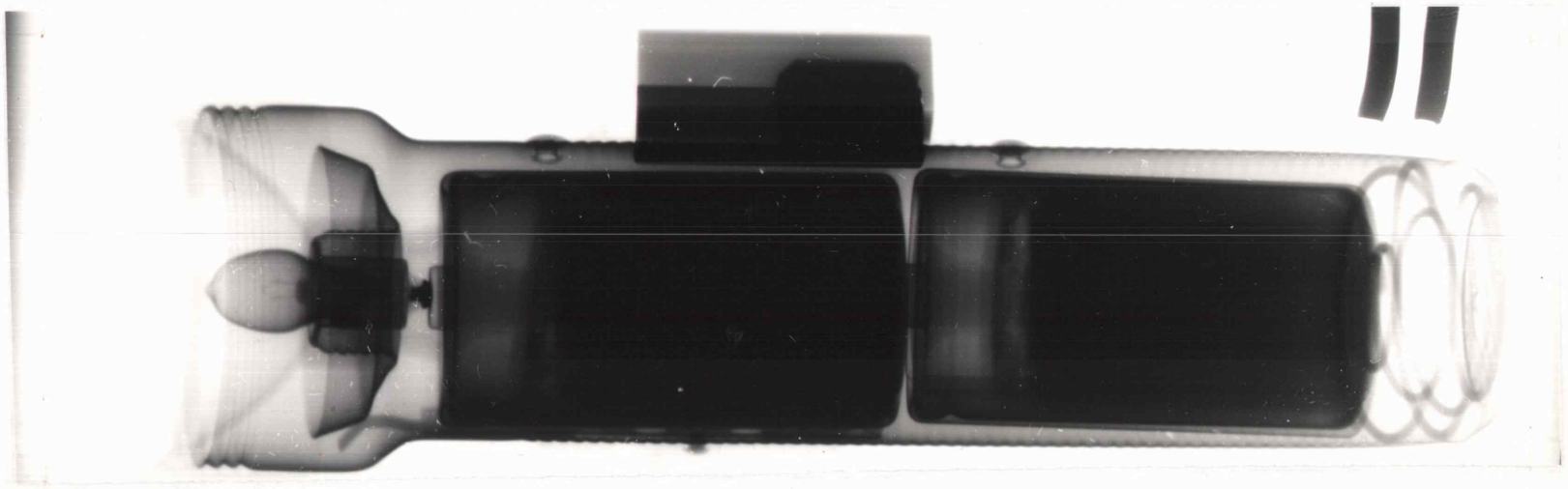

Figure 2.3 X-radiograph of Flashlight

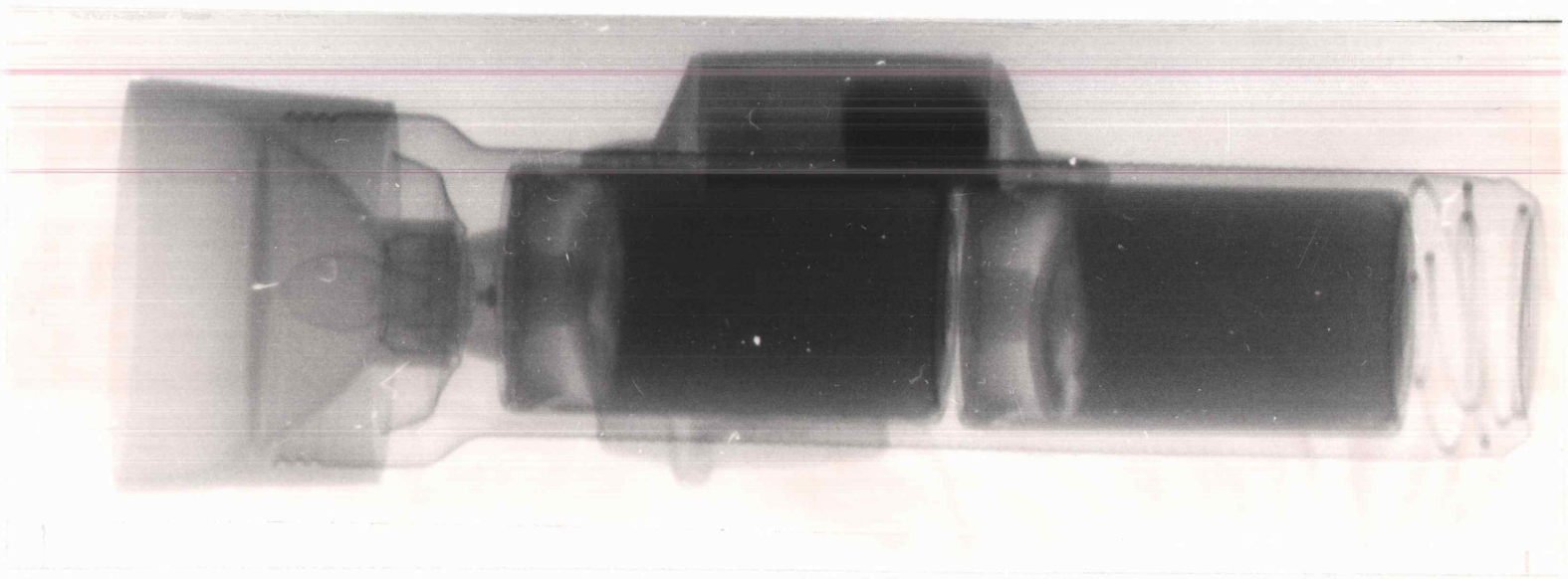

Figure 2.4 Gamma Radiograph of Flashlight

Another example is shown in the images of some bullets. Figure 2.5 shows the positive print of the neutron radiograph while Figure 2.6 shows the positive print of the X-radiograph of the bullets. These pictures show that the powder of the bullets can be seen much more clearly in the neutron radiograph than in the X-radiograph.

UO_2 fuel pins were radiographed by neutron radiography and by gamma radiography. Some details such as cracks, fractures, or different enrichments of the fuel pellet type, can be seen from these two methods. However, the neutron radiograph shows much more detail and much better overall visibility than the gamma radiograph. The description of the fuel pins and various radiograhic methods results of special UO_2 fuel pins will be dealt with in more detail in chapter IV.

Some objects, such as irradiated fuel pins which might not be suitable for X-radiography, can be radiographed using neutrons or gamma rays. But, some objects, such as OSU TRIGA fuel elements, which contain U-$ZrH_{1.7}$, cannot be radiographed with neutron radiography, but can be successfully radiographed with gamma rays. The description of OSTR fuel elements will be given in chapter III, and the results of various radiographic techniques will be discussed in chapter V.

Air or vapor bubbles rising through water (light or heavy) while inside a steel box (46), or the slow movement

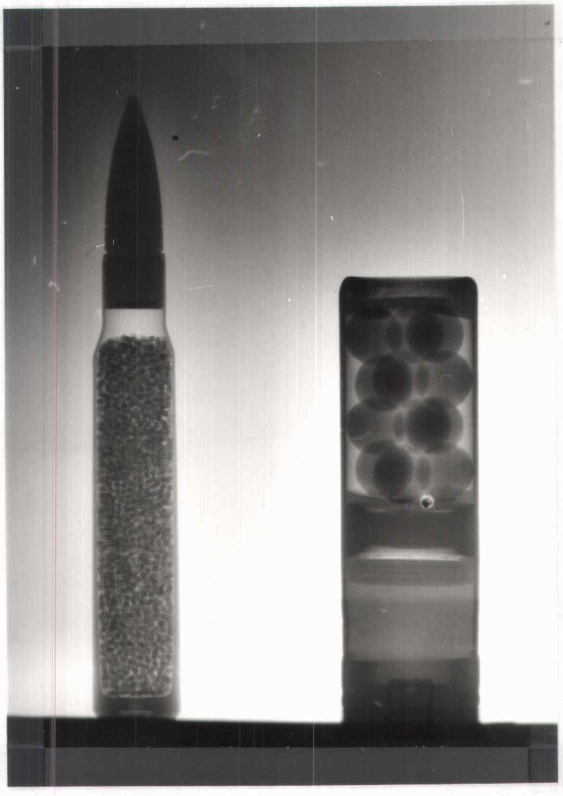

Figure 2.5 Neutron Radiograph of Bullets

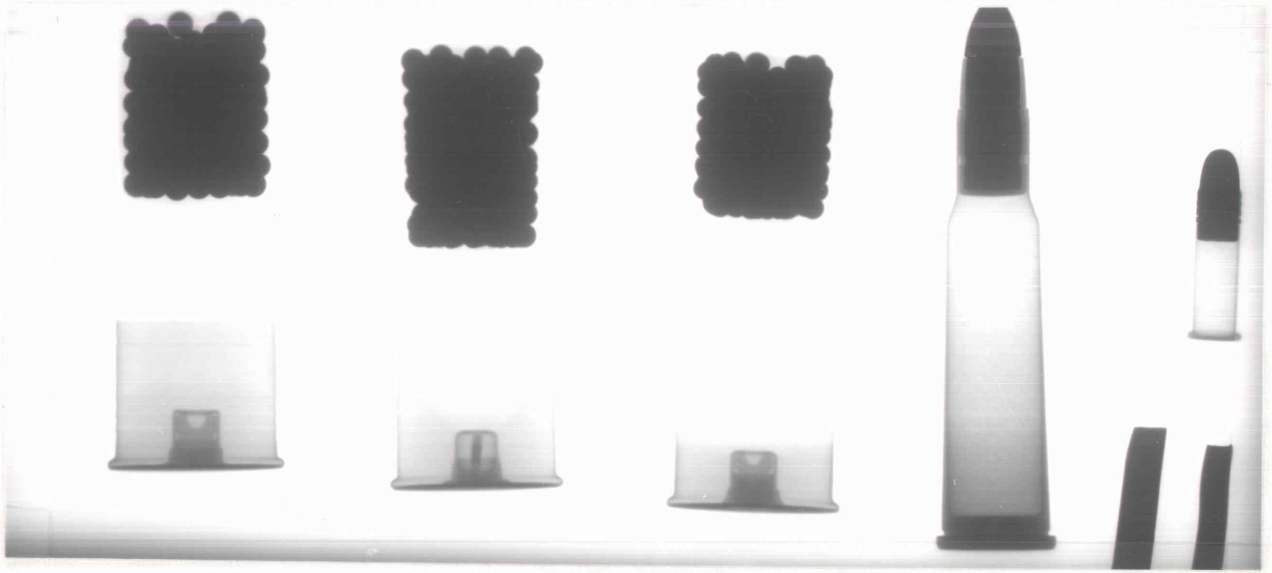

Figure 2.6 X-radiograph of Bullets

of an object such as a pencil inside a steel casing swinging on a thread can be successfully neutron radiographed by using pulsed radiography. The latter event was done at OSU (47) in order to estimate the amount of blurring which could occur from the unexpected motion of a stationary object over the length of the pulse. The recoil of a rifle barrel during the firing of cartridges has also been observed by using pulsed radiography and high speed motion neutron radiography (47).

2.4 Cassette

A cassette is used to hold the imaging film or converter screen or both during the radiographic exposure. For X- and gamma radiography only the film is in the cassette. For neutron radiography the film and converter screen must be held in contact with each other during the exposure. The resolution capability of the system is significantly improved by a tight contact between the film and the converter screen. For this reason vacuum cassettes are the best for stationary neutron radiography. The resolution of the system also depends on the materials used to construct the cassette. This situation is illustrated in the gamma radiogrpahs taken of the TRIGA fuel. All of the pictures taken with a metal cassette give excellent results. However, such excellent results cannot be obtained using cassettes with a plastic cover. This is due to the fact that the materials in the plastic cover have variable densities. The transmission of gammas through the plastic cover results in different background darkness on the film. These patterns on the film are so randomly distributed that one cannot tell what those patterns mean and what the dark areas or light areas mean. Thus, the imaging of real defects, cracks, and inclusions are disguised by the cassette pattern. Trouble from spurious patterns can also be caused by certain materials in front

of the object, such as cadmium. An attempt was made to cut out the thermal neutrons by using cadmium in order to raise the ratio of gammas to neutrons in the beam by putting a cadmium sheet in front of the TRIGA fuel. These films were fogged and an unexpected pattern appeared in the picture, even using a metal cassette. Using a plastic cassette made the situation even worse. The explaination is that the image of the cadmium is superposed on the image of the plastic or the metal cassette. The cadmium sheet not only cuts the thermal neutrons off, but it also decreases the intensity in the gamma rays of the beam. So for gamma radiography, it is best to put nothing in front of the film cassette.

2.5 Neutron Imaging

X-radiography or gamma radiography uses a photographic film placed behind the object to record the emergent radiation pattern. This is not possible in neutron radiography, since photographic films are very insensitive to neutron radiation. Therefore, converter foils or scintillator screens are used to convert the neutron image into a recordable ionizing radiation or light image.

The nuclei in a neutron converter foil absorb a fraction of the spatially modulated transmitted neutron image beam from the object and release some form of ionizing radiation, usually beta and/or gamma radiation.

Many types of converter screens exist, each with different characteristics of sensitivity and sharpness. The most useful converter screens for thermal neutron image detection are gadolinium and dysprosium. Indium foils are very useful for epithermal neutron radiography.

Gadolinium metal sheets or vapor-deposited gadolinium imaging screens can be obtained in a varity of sizes and thickness. The relative natural abundance of ^{155}Gd is 14.73%, and the reaction of ^{155}Gd with thermal neutrons is

$$^{155}Gd + n \text{ --- } ^{156}Gd + \gamma$$

The thermal cross section of ^{155}Gd is 61,000 barns. Neutrons absorbed in gadolinium generate internal conversion

electrons, which in turn directly expose the film. This technique, using a one mil gadolinium foil or a 25 μm vapor-deposited gadolinium layer and fine grain film, presently provides the highest quality neutron radiographs.

After studying the resolution of the converter screens, Berger (4) pointed out the superiority of gadolinium for optimum radiographic resolution. The excellent resolution qualities of this material appear to be due to a combination of a very high neutron cross section, a fact which permits the use of very thin screens with reasonable exposure times, and the fact that gadolinium emits some very soft and easily absorbed radiation upon neutron bombardment. Gadolinium screens 0.00025 to 0.0005 inches thick can resolve line images separated by distances as small as 0.0004 inches when used with medium or slow speed X-ray films (4). This corresponds to a resolution of 49 line pairs per millimeter (lp/mm). However, compromises between speed and resolution must be made. Berger (4) indicated that the relative speed of single Gd screens will drop off very rapidly as the screens become thinner. Generally speaking, the thinner the screens are the better the resolution. The thicker the screens are, the faster the speed.

Indium and dysprosium screens are also frequently used in neutron radiography. The relative natural abundance of indium-115 is 95.97% and dysprosium-164 is 28.1%. The

reaction of ^{115}In with neutrons is:

$$^{115}In + n \text{-----} ^{116m}In$$

the reaction of ^{164}Dy with neutrons is

$$^{164}Dy + n \text{-----} ^{165m}Dy$$

Indium-115 has a thermal neutron cross section of 155 barns, and has a half-life of 54 minutes. A diagram of the total cross section of indium versus neutron energy is shown in Figure 2.7. The thermal neutron cross section of Dysprosium-164 is 500 barns. Its half-life is 1.25 minutes. Both of these converter screens are used with the transfer method of imaging.

Light emitting converter screens, called scintillators, offer an alternative to metal screens. Such scintillators offer much higher speed than metal screens but at the sacrifice of resolution. The resolution of scintillators is seldom above a few lp/mm.

Scintillator screens contain a high neutron absorption cross section material such as ^{6}Li, ^{10}B or ^{155}Gd plus a scintillation material. Following neutron absorption, the scintillation material, such as zinc-sulphide, is stimulated by charged particles from the neutron interaction and light is emitted (Figure 2.8). The light may be used to expose light sensitive film or input into other optical devices.

The lithium fluoride-zinc sulphide screens are most widely used due to their high yield, ease of manufacture

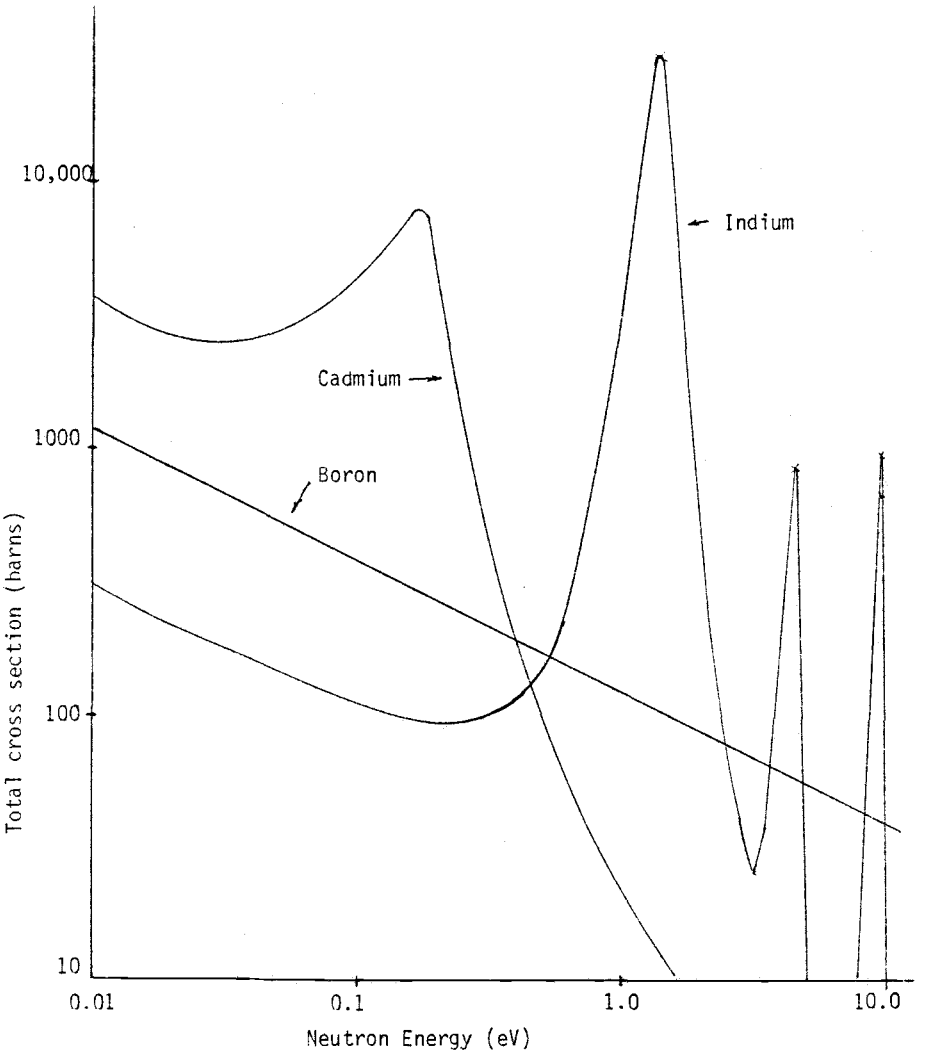

Fig.2.7. Variation of the total neutron cross section versus neutron energy for boron, cadmium,and indium.

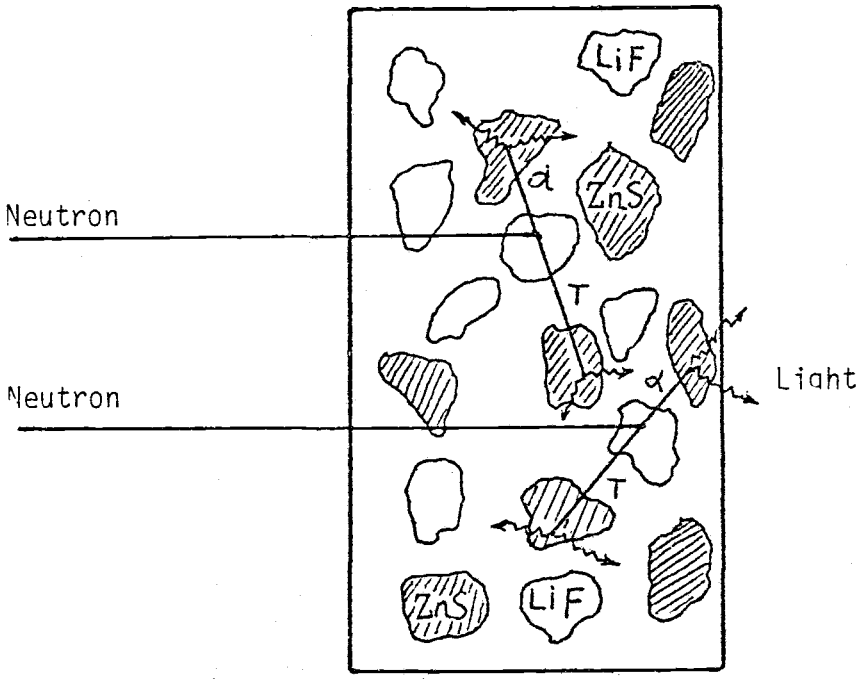

Fig.2.8. LiF-ZnS Scintillator

and durability. The composition of these screens is of a mixture of LiF powder and ZnS powder with a binder material. A binder of polyethylene, plastic, lucite, epoxy, sodium silicate or other appropriate material is required to hold the LiF and ZnS powder together in the mixture and usually, though not necessarily, to an aluminum substrate. The composition of LiF is enriched in its content of ^{6}Li to 95% or more. Lithium has a neutron absorption cross section of 953 barns. When lithium absorbs neutron and it splits into two particles, an alpha particle and tritium nucleus, releasing 4.78 MeV of energy. The reaction is:

$$^{6}Li + n \text{ --- } \alpha + {}^{3}H + 4.78 \text{ MeV}$$

2.05 MeV of the energy will be carried away by the alpha and 2.73 MeV by the triton. These two particles will travel through the scintillator losing their energies by excitation and ionization. If the particles happen to excite the ZnS crystals, light scintillation at about 450 nm wavelength will occur as the lattice returns to the ground state.

The criteria for selecting suitable scintillators are the light yield, resolution capability and the rate at which the light decays from the scintillator. Comparisons of the relative yield and image quality of various scintillators can be found in Bossi's thesis (50). Bossi reported that LiF-ZnS screens have image good quality and are the

fastest type of scintillator screen (i.e. maximum light yield). And he also pointed out that B-10-Zinc sulphide screens are slower and have markedly poorer image quality. Gadolinium rare earth screens demonstrated the best image quality but do not have a great light yield. Glass scintillators have image qualities comparable to the LiF-ZnS screens but one of the poorest light yields.

Scintillators may be easily made without a great deal of difficulty in the laboratory. The procedure for scintillator construction can be found in Bossi's thesis (50) and Tollefson's thesis (47). The weight ratio of LiF to ZnS is very important for both sensitivity (light yield) and resolution. The best LiF-ZnS scintillators were constructed with a weight ratio of 2 parts of ZnS to 1 part of LiF.

The scintillator analysis by Bossi and Robinson (52) shows that a LiF-ZnS scintillator is presently the type of scintillator best suited for high speed motion neutron radiography work in the range of 2000 to 10,000 frames/sec. At lower frame rates rare earth scintillators may be better for their superior image quality.

As a summary, for direct stationary neutron radiography a 25 μm vapor-deposited gadolinium foil is the best detector. For the thermal transfer method, dysprosium foil will yield the best results. Indium converter screens are recommended for epithermal neutron radiography. LiF-ZnS

scintillator screens are best suited for high speed motion neutron radiography work or other application requiring a minimum of neutron exposure.

III. DESCRIPTION OF THE OSU TRIGA REACTOR

3.1 OSTR Characteristics and Pulsing Mode Operation

The Oregon State University TRIGA Reactor (OSTR) is a training and research TRIGA Mark II nuclear reactor manufactured by the General Atomic Company of San Diego, California (48,49). The OSTR is licensed for steady state operation at a maximum thermal power of 1 MW, and for pulsing operation to a maximum power of approximately 3000 MW (the license limit is on the reactivity inserted). This pulsing operation is essential for high speed motion neutron radiographic applications.

A standard OSTR fuel-moderator element is shown in Figure 3.1. The active section of the fuel element is 15 inches long and 1.43 inches in diameter. To facilitate hydriding a 0.25 inches diameter hole is drilled from both ends of the fuel element through the center of the active section. A zirconium rod is inserted in this hole after hydriding is completed. Graphite cylinders 3.44 inches long and 1.43 inches in diameter are used as axial reflectors in the fuel element. The fuel and graphite reflectors are clad in a 0.020 inches thick stainless steel tube.

The standard TRIGA element, which has a gap of only 1 or 2 mils between the fuel and the cladding, is slip-fit

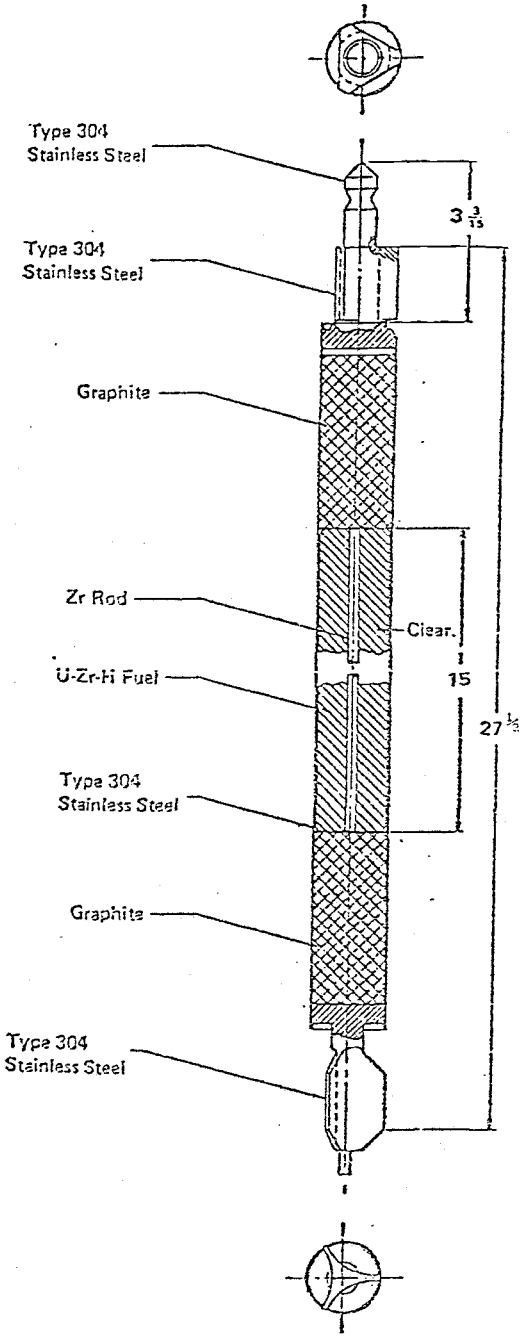

Fig.3.1 Typical TRIGA fuel element.

together and contains 8.5 w/o uranium of which 20 w/o is uranium-235.

The recently developed Fuel Lifetime Improvement Program (FLIP) fuel, which contains 70% enriched ^{235}U, contains up to 1.6% erbium as a burnable poison to increase the core lifetime in the higher power (1-to 14 -MW) TRIGA reactors (42,43). The addition of erbium to the U-$ZrH_{1.7}$ introduces no deleterious effects to the fuel. Erbium has a high boiling point and a relative low vapor pressure so that it can be melted into the uranium-zirconium uniformly.

An instrumented fuel-moderator element contains three thermocouples embedded in the fuel. As shown in Figure 3.2, the sensing tips of the thermocouples are located halfway between the outer radius and the centerline of the fuel section. One thermocouple is located at the mid-plane level with the others one inch above and below the mid-plane. The thermocouple leadout wires pass through a seal contained in a stainless steel tube welded to the upper end fixture. This tube projects about 3 inches above the upper end of the element and is extended by two 10-foot lengths of tubing connected by unions to provide a watertight conduit carrying the leadout wires above the water surface in the reactor pool. In other respects, the instrumented-fuel element is identical to the standard fuel element. Figure 3.3 shows fueled-follower-type control rod. The upper section of the control rod is graphite; the

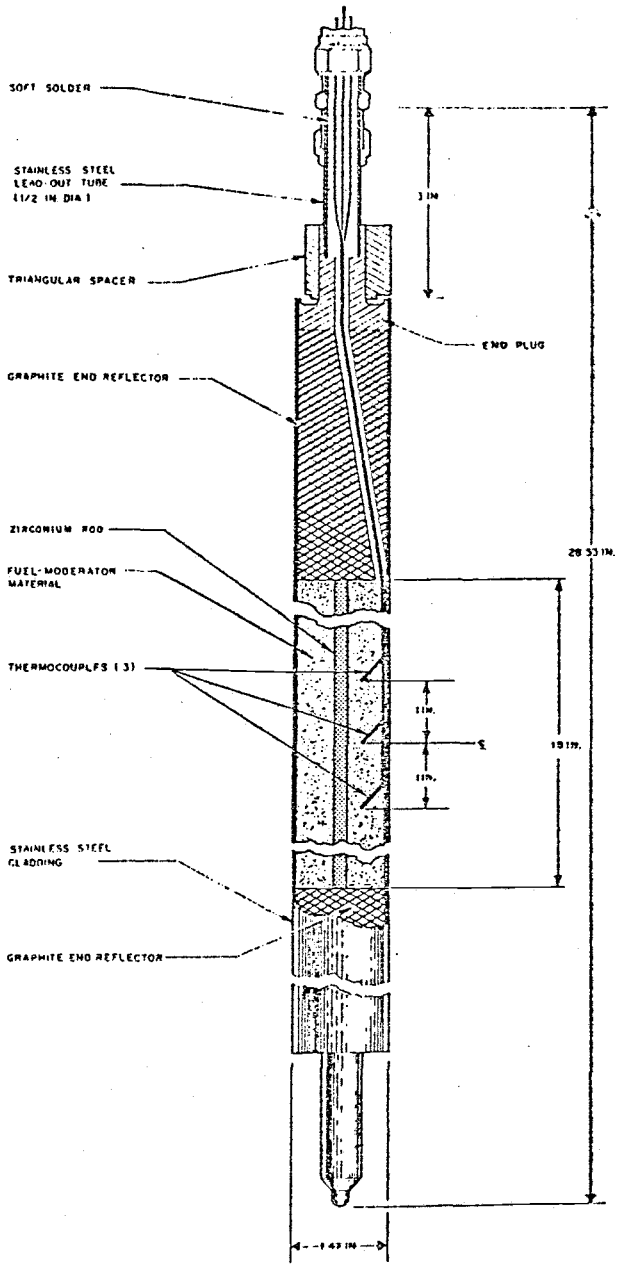

Fig. 3-2 --TRIGA reactor instrumented fuel element

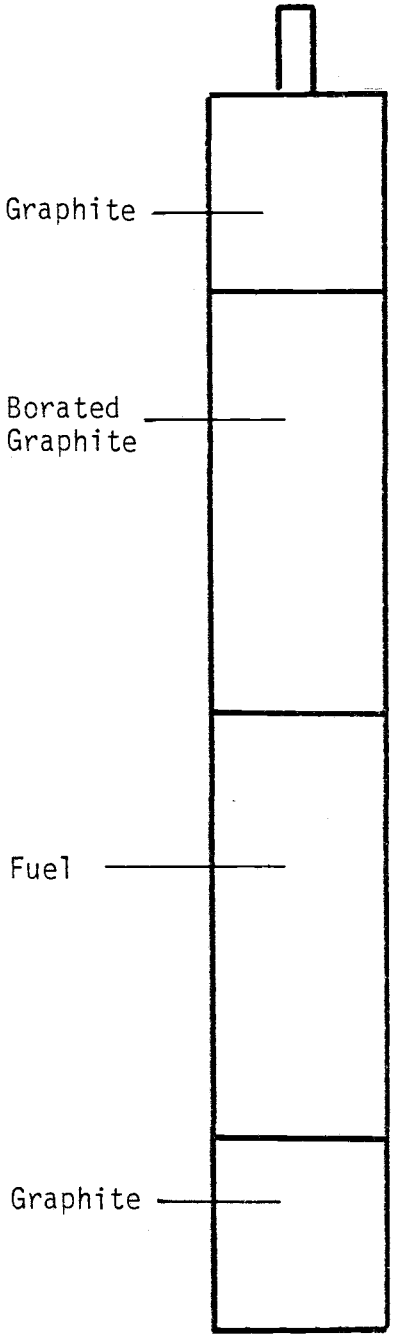

Fig.3.3 Fueled-follower-type Control Rod

next 15 inches is the neutron absorber (graphiter impregnation with powered boron carbide); the follower section consists of 15 inches of U-$ZrH_{1.7}$ fuel with a zirconium rod through the middle; and the bottom section is graphite.

The other basic parameters of the OSTR are as follows:

1) Hydrogen-to-zirconium atom ratio in the fuel element is 1.68 to 1 (average).
2) Cladding is 0.020 inch thick 304 stainless steel.
3) The overall length of the fuel element, 28.37 in.
4) The outside diameter of the fuel element, 1.47 in.
5) Fuel composition, U-$ZrH_{1.7}$.
6) Weight of ^{235}U, 38 grams (average for standard fuel); FLIP has 3.5 times as much.
7) Cold, clean critical loading: 59 elements, 2.244 Kg uranium-235.
8) Operation loading: 90 elements, 3.4 Kg ^{235}U.
9) Four control rods: a regulating rod, a shim rod, a safety rod, and a transient rod.
10) Maximum cold, clean excess reactivity: $ 7.00 (4.9% $\Delta K/K$).

The safety of the TRIGA reactor lies in the large prompt negative temperature coefficient that is an inherent characteristic of the uranium-zirconium hydride fuel-moderator material. Thus, even when large sudden reactivity insertions are made and the reactor power rises on a

short period, the excess reactivity is compensated automatically because the fuel temperature rises simultaneously so that the system returns quickly to normal power level before any heat is transferred to cooling water. Both the standard and the FLIP types of fuel available for use in TRIGA reactors are specially designed to have a large prompt negative temperature coefficient of reactivity which reduces the fission rate in the fuel at high temperatures. It is this reactivity feedback mechanism that allows the TRIGA to operate routinely and safely in the pulsing mode.

The location of the control rods and a typical fuel loading pattern, as well as the location of the central thimble and the concentric ring circular grid pattern of the OSTR are shown in a core map such as the one in Figure 3.4.

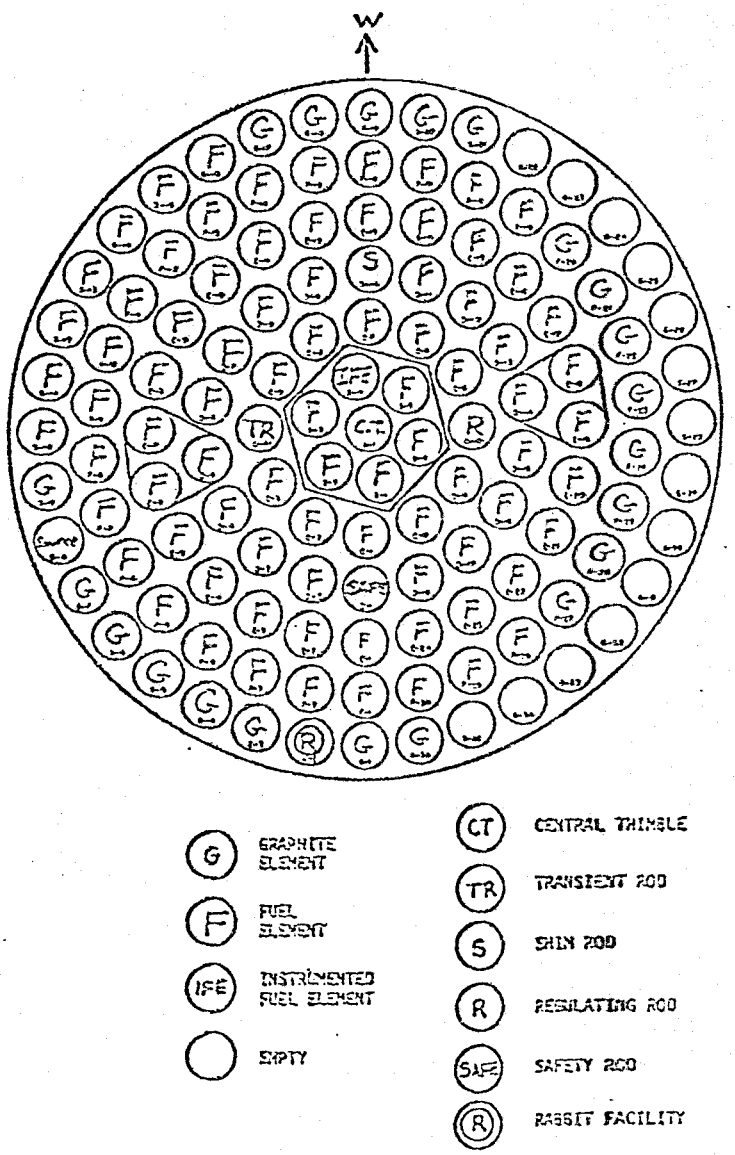

Figure 3.4. OSTR Core Map and Typical FLIP Fuel Loading Pattern.

3.2 Beam Port Facilities

The OSTR facility is equipped with four beam ports. These ports consist of air filled tubes piercing the reactor shield which allow neutrons from the core to reach experimental facilities outside the shield. Each beam port has a slightly different configuration. This determines the energy distribution of the gamma rays and neutrons exiting the individual ports. The quality of the beam for radiography is determined by the beam port configuration and collimators placed in the beam tube. In a later section a method of quantifying the beam quality is presented. Beam quality is measured with a " beam purity indicator".

Static radiography is performed using beam port #1 because this beam port has collimators which can provide length to diameter ratios between 100:1 and 600:1. This high degree of collimation provides very high resolution in neutron radiographs, the resolution being better than 40 lp/mm. The design of the beam port #1 facility allows static neutron radiographs to be taken without affecting the normal operation of the OSTR.

The relative location of beam port #1 to the reactor core is shown in Figure 3.5. Figure 3.6 shows the neutron radiography facility adjacent to beam port #1. This beam port uses a two piece collimator which produces the effect

Fig.3.5 BEAM PORT #1 NEUTRON RADIOGRAPHY FACILTIY

(scale 1mm = 1 inch)

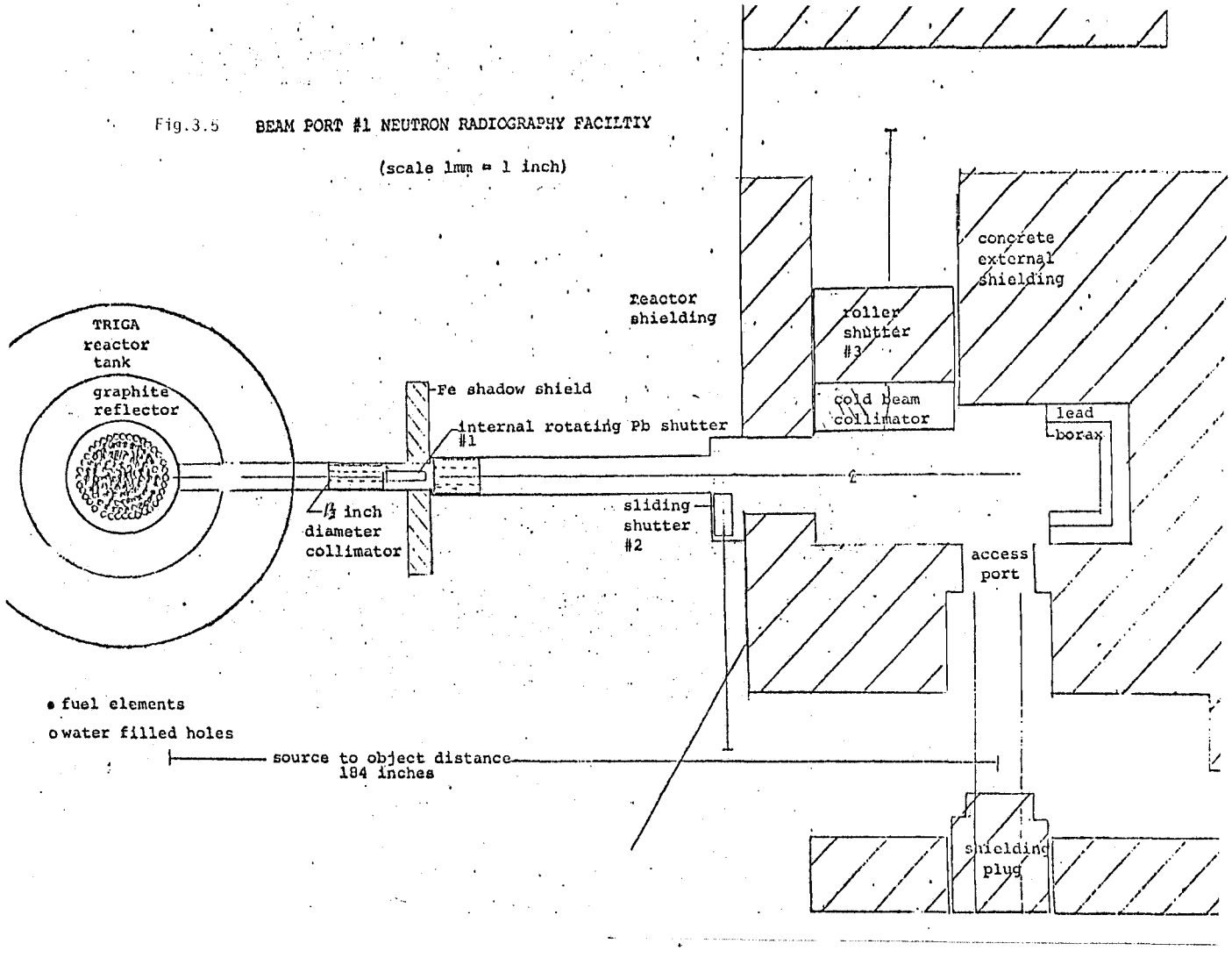

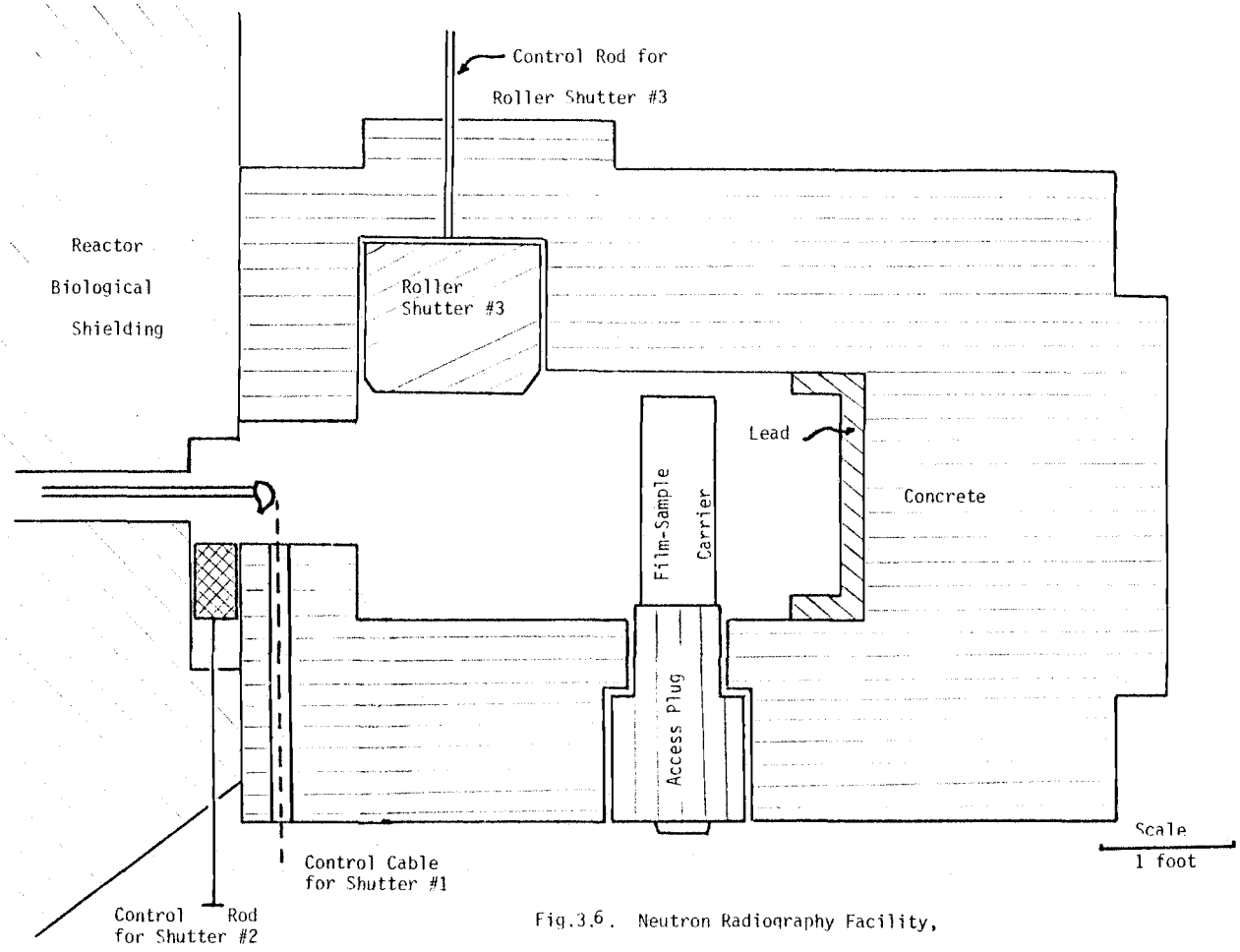

Fig.3.6. Neutron Radiography Facility,

Beam Port #1

of a point source of neutrons. The beam produced by this collimator is the same as would be produced from a source placed in the center of the collimator. The effective diameter of the source is just the collimator's diameter at its smallest aperture. The shutters are shown in Figure 3.7, and the collimator is shown in Figure 3.8. The collimator normally contains a neutron aperture insert constructed of Pb-Cd-In alloy which is placed in the center of the aluminum canned (Pb-Cd alloy and masonite) primary collimator. This entire collimator (with aperture insert) is situated near the inner end of the beam port on line with the outer edge of the TRIGA pool. All the thermal neutrons and most of the fast neutrons and gamma rays leaving the beam port have to pass through the collimator aperture. Additional shielding is placed in the beam port at the junction of the 6 to 8 inches diameter sections to guarantee removal of all radiation except that passing through the aperture. This divergent beam of neutrons exits from the face of the reactor biological shield through beam port #1 into a cavity in a concrete block-house. This cavity contains the object to be radiographed, the neutron converter and film, and also acts as the beam catcher and biological shield.

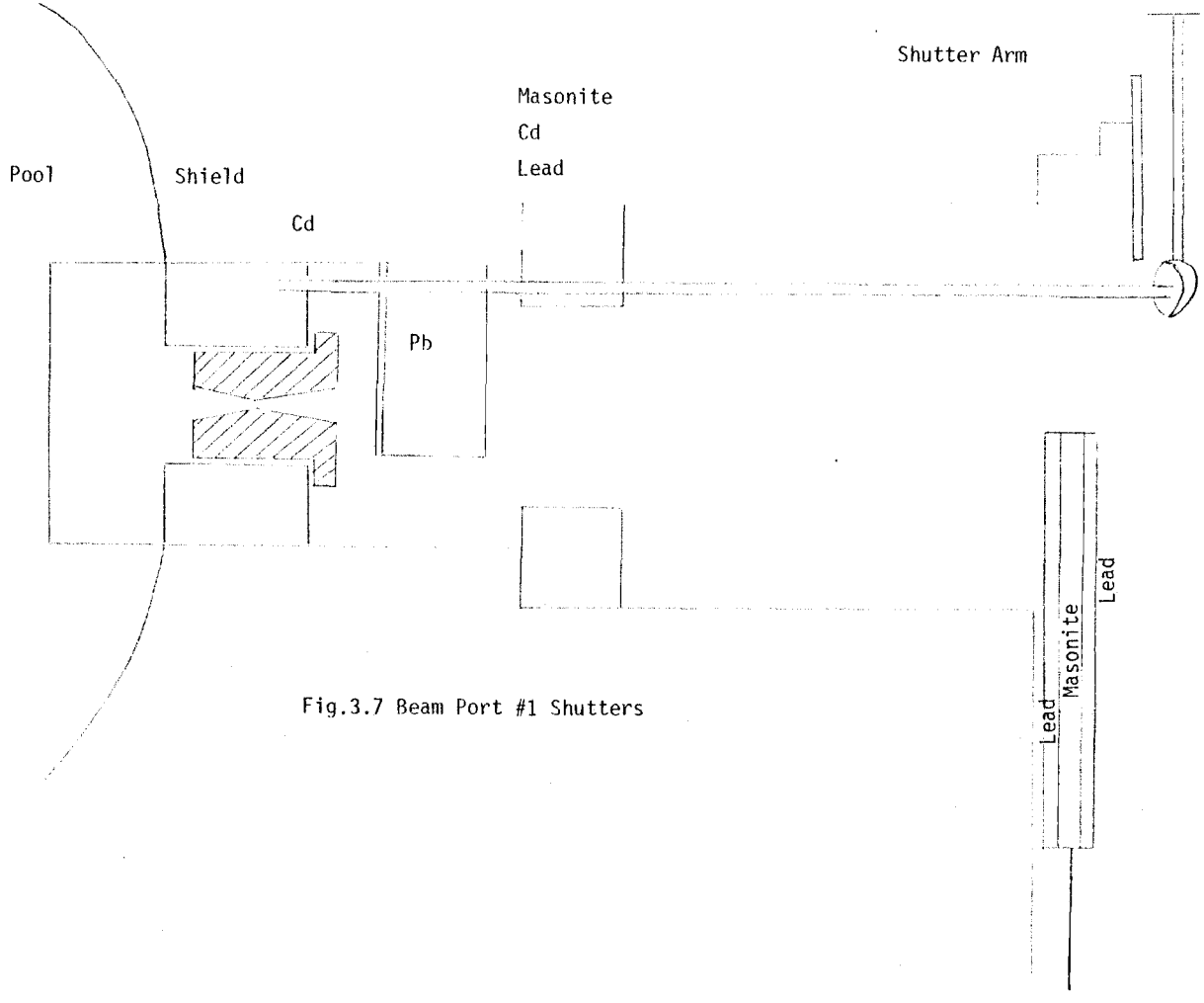

Fig.3.7 Beam Port #1 Shutters

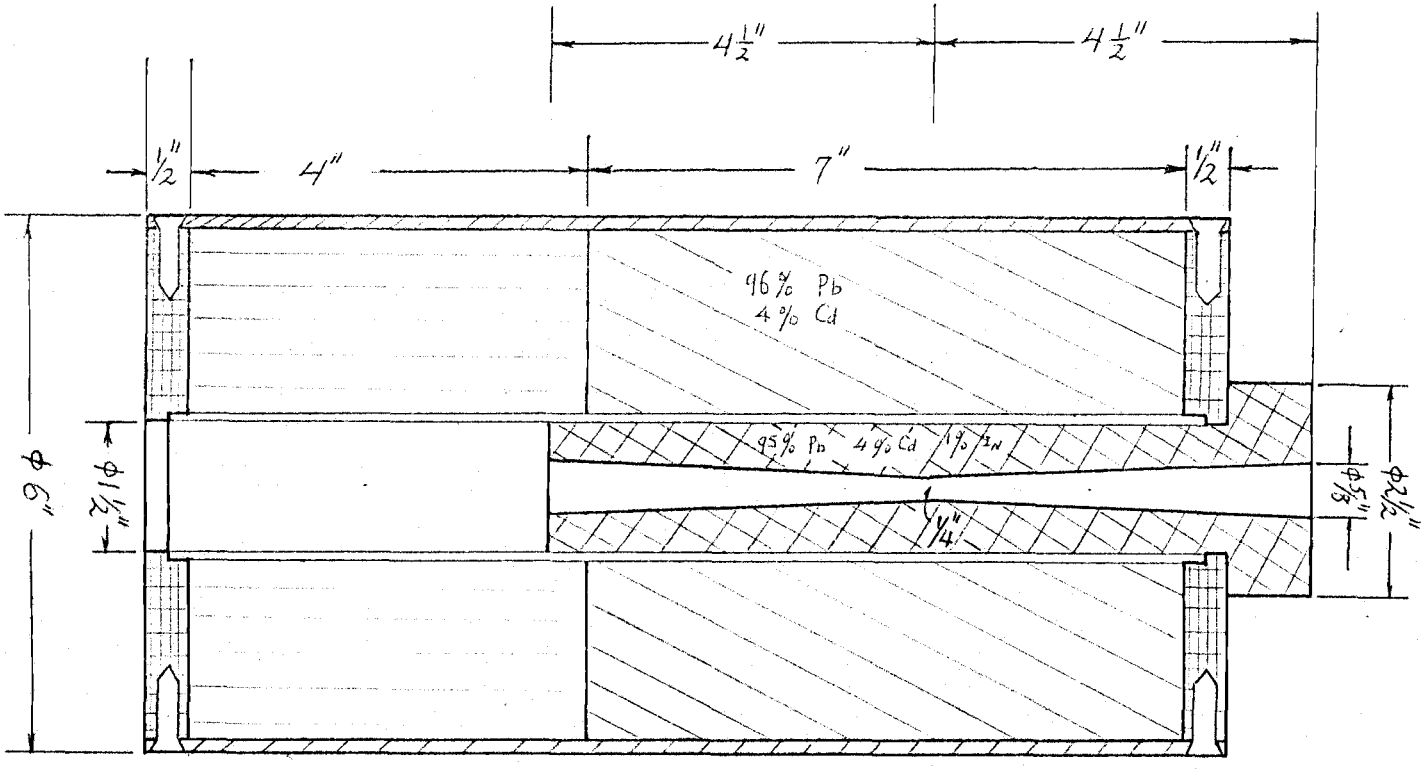

Fig. 3.8 Beam Port #1 Collimator

3.3 Neutron Beam Quality

The quality of the beam used for neutron radiography can be evaluated by making use of the images obtained from indicators which are exposed along with a test object. There are two basic indicators. One is the beam purity indicator, as shown in Figure 3.9. This beam purity indicator is now the standard of the ASTM. It consists of a section of boron nitride with three drilled holes. One hole contains a disc of boron nitride; another contains a disc of boron nitride plus lead, and the remaining hole is open. By making the proper densitometric mearsurements of the radiographic image of beam purity indicator, the relative amounts of thermal neutrons, scattered neutrons, epithermal neutrons, and low energy gamma rays in the beam can be determined. The results of such a measurement for beam port #1 are listed in Table 3.1. The second method of determining the quality of a beam is to use the image quality indicator (IQI) shown in Figure 3.10. It is based upon the detection of holes in machined, cast acrylic step wedges. The sensitivity level or quality of the image is determined by the smallest observable hole and thickness of the corresponding absorber in the indicator.

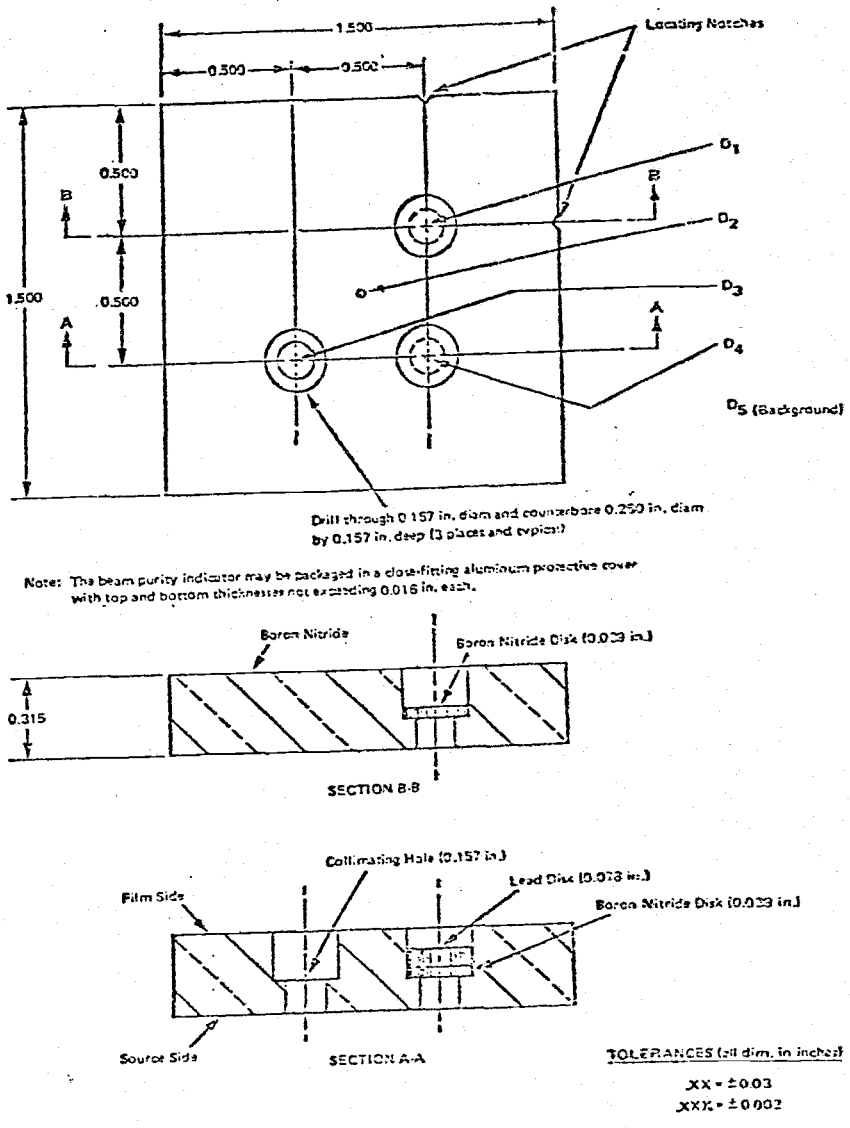

Fig.3.9 BEAM PURITY INDICATOR (all dimensions in inches)

TABLE 3.1 ASTM BEAM PURITY INDICATOR

Location	Film Density*
D1	.35
D2	.29
D3	1.45
D4	.32
D5	1.56

$\frac{D3-D1}{D3}$ (thermal neutron content) = .76

$\frac{D5-D3}{D3}$ (scattered neutron content) = .08

$\frac{D1-D2}{D3}$ (epithermal neutron content) = .04

$\frac{D1-D4}{D3}$ (low energy gamma content) = .02

* Exposure on gadolinium foil - SR film

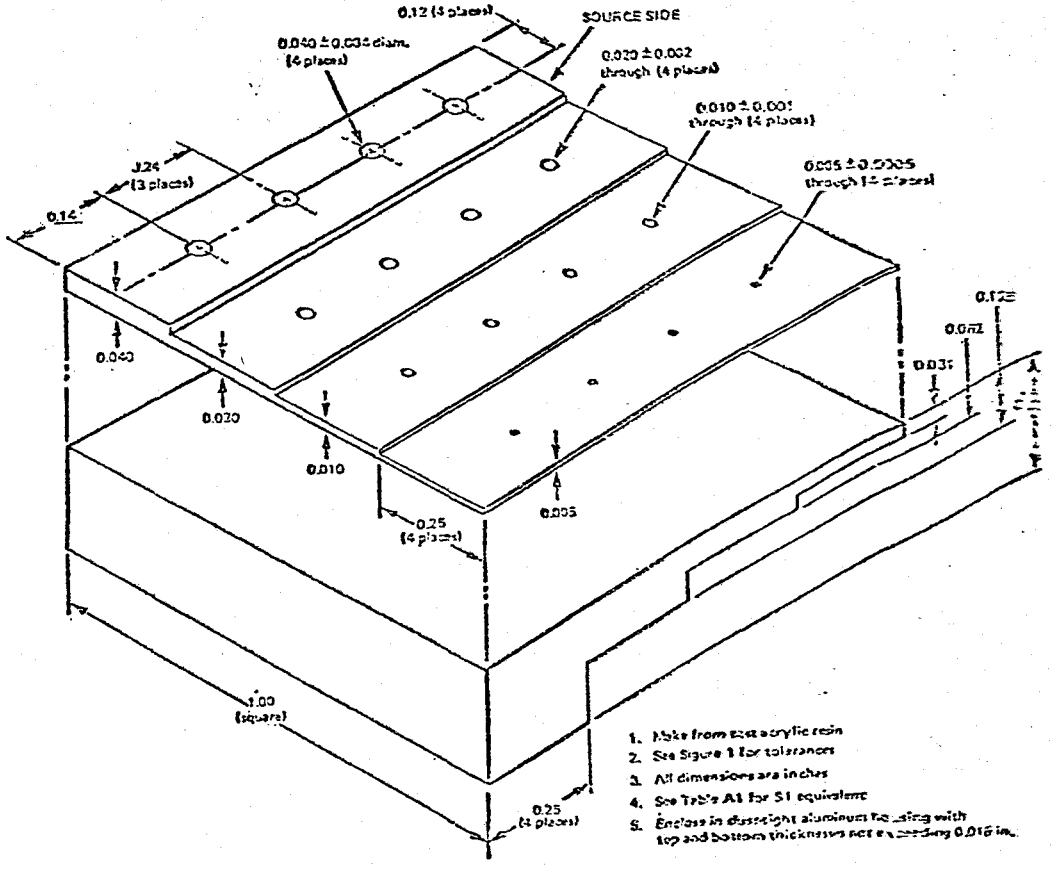

Fig.3.10 TYPE A SENSITIVITY INDICATOR

IV. RADIOGRAPHY OF UO_2 FUEL PINS

4.1 Introduction

In this chapter the results obtained from the radiography of the special UO_2 fuel pins are presented. The next chapter presents the results obtained for the TRIGA fuel.

In order to determine the applicability of neutron radiography to the detection of defects in nuclear fuel, seven special UO_2 fuel pins were constructed with known defects. Examples of these defects are alumina inclusions, cracks, chips, enrichment errors, size errors, and position errors.

The UO density in the fuel pellets of these special pins is 10.5 g/cm^3 . The enrichment in ^{235}U (wt%) varies, but it is about 3 w/o in each pin. The cladding material is 0.6 inches diameter zirconium tubing. The pellets are held in place by steel springs pressing on alumina (Al_2O_3) spacers. Each pin contains about 20 pellets and each has a variety of internal defects.

This study is concerned with the ability of neutron and gamma radiography of fuel to provide information about the internal conditions of the fuel.

Neutron and gamma radiographs were taken of the special UO_2 fuel pins using the facilities on beam port #1. It

was found that by using neutron and gamma radiography for inspecting these fuel pins all the known defects were observable. Additionally, some unexpected defects were also observed. The best results were obtained by using the direct stationary neutron radiography with vapor-deposited gadolinium in a vacuum cassette. The indium foil transfer method and epithermal neutron radiography were also employed for inspecting special fuel pin 7, and good results were obtained.

4.2 Neutron Radiography of Special UO_2 Fuel Pins

4.2.1 Direct Neutron Radiography of Special Fuel Pins

For direct neutron radiography, these seven fuel pins were mounted on a vertical aluminium rack and radiographed in a single exposure. During each exposure the fuel pins were held in the vertical position and subjected to an integrated thermal neutron exposure of 7.2×10^9 n/cm^2. Using a vapor-deposited gadolinium converter screen (10 by 8 inches) and DR-5 double emulsion Kodak X-ray film such an exposure required 4 minutes total exposure time to obtain high quality radiograph.

In the following, the radiographic pictures are presented to show examples of the principal defective conditions observed. Each condition is followed by a description of the result of examinations that indicate the nature and extent of the defect.

Figure 4.1 shows a positive print of all seven fuel pins. It is convenient for us to number these pins and pellets. The top pin is numbered pin 1, the bottom is numbered pin 7. The left hand pellet of each pin is number 1, and the number for each pellet is increased from left to right.

As shown in Figure 4.1, pin 1 has 20 pellets, 11 of correct size. The nearly transparent pellets are alumina

Figure 4.1 Neutron Radiograph of UO_2 Fuel Pins (Taken at 0 degree)

(used as spacers in LWR fuel designs). The pin contains three spacers. Pin 2 has 22 pellets, none of them of correct size, and three spacers. Pin 3 has 19 pellets, none of them of the correct size, and 5 spacers. Pin 4 has 17 pellets, among them, twelve of the correct size, and five alumina spacers. Pin 5 has 17 pellets, all of them at the correct size, and three spacers. Pin 6 has 19 pellets, among them, five of the correct size. One pellet was put in on its side. The pin also contains 4 spacers. Pin 7 has 17 pellets, among them, 9 of the correct size, the other pellets are undersized. One pellet was put in on its side, and there are five spacers.

Thermal neutrons are highly attenuated by enriched fuel, thus, the radiographs show a high contrast between the fuel and nonfuel regions. The image density variation from pellet to pellet, for pellets of the same diameter, is caused by small variations in enrichment. Thus, the image density of a pellet containing more UO_2 is darker than that of a pellet containing less UO_2.

Portions of a pellet that exhibit relatively large physical density changes can be readily detected as shown at pellets 5, 6, and 8 of pin 4 in Figure 4.1. In this case, a sizable lamination and associated void volume in each pellet are readily evident in the neutron radiograph. These laminations extended more than halfway around these pellets. There are also two laminations in pellet 3 of pin

1, one at the left end of this pellet, the other at the right end. These two laminations extended all the way around this pellet. The same phenomena can be observed in pellets 4 and 5 of pin 1, pellets 11 and 12 of pin 6, and pellet 13 of pin 7. Many smaller laminations can also be detected. When many small laminations occur very close to each other in a single pellet, the neutron radiographic image appears as a speckled pattern of dark spots corresponding to the small voids present. The neutron beam fully penetrates the fuel and provides a complete and detailed image of the relatively small void volumes. This may be seen in pellets 5 through 10 of pin 7. Small void volumes can also be found in pellets 5 through 17 of pin 5.

The previous discussion for laminations also applies to the structural flaws shown in pellets 4 and 12 of pin 7. The primary difference is that the flaw is oriented nearly parallel, rather than perpendicular, to the pellet axis and constitutes a structural flaw. A bright area shown in pellet 4 of pin 5 indicates a large void volume contained in the middle of this pellet. Cracks can also be seen in the neutron radiographs. Pellet 4 of pin 7 is not only structurally flawed but also cracked seriously. Pellet 12 of pin 7 was smashed very seriously. The smashed pieces and associated cracks, laminations, structural flaws, and voids can be clearly seen in the image of this pellet.

In order to estimate the location of voids or the size

of defects, pictures having a different rotational orientation of the fuel pins with respect to the neutron beam have been taken. Every special UO_2 fuel pin has a serial number at the top end (not radiographed). The rotation of every fuel pin is assigned to be zero in direction when the number of that pin is facing the neutron beam. Figure 4.1 shows that the pins were taken at the zero degree rotation. Figures 4.2 and 4.3 show the radiographs taken at 45 and 135 degrees, respectively. These pictures are also positive prints. The advantage of changing the rotation of fuel pins is that the dimension of a defect, crack, or void and the location of laminations and structural flaws can be approximately estimated. Pellet 11 of pin 6 appears to have no defects in Figure 4.1 or 4.3, except that it is in an incorrect position. It might be mistaken for a good pellet. However, after changing the rotation of the pin for another neutron radiograph, laminations can be seen in this pellet. This is shown in Figure 4.2, which was taken at the 45 degree roational position. The same discussion holds for pellet 13 of pin 7. From the 45 degree picture (Figure 4.2), it appears that the void and chip defect of pellet 4 of pin 5 are connected together, but actually they are not. If they were, the connection would be observed in all rotations. The separated image of the void and chip defect in this pellet can be found in the zero degree rotation picture (Figure 4.1). A big defect can be seen

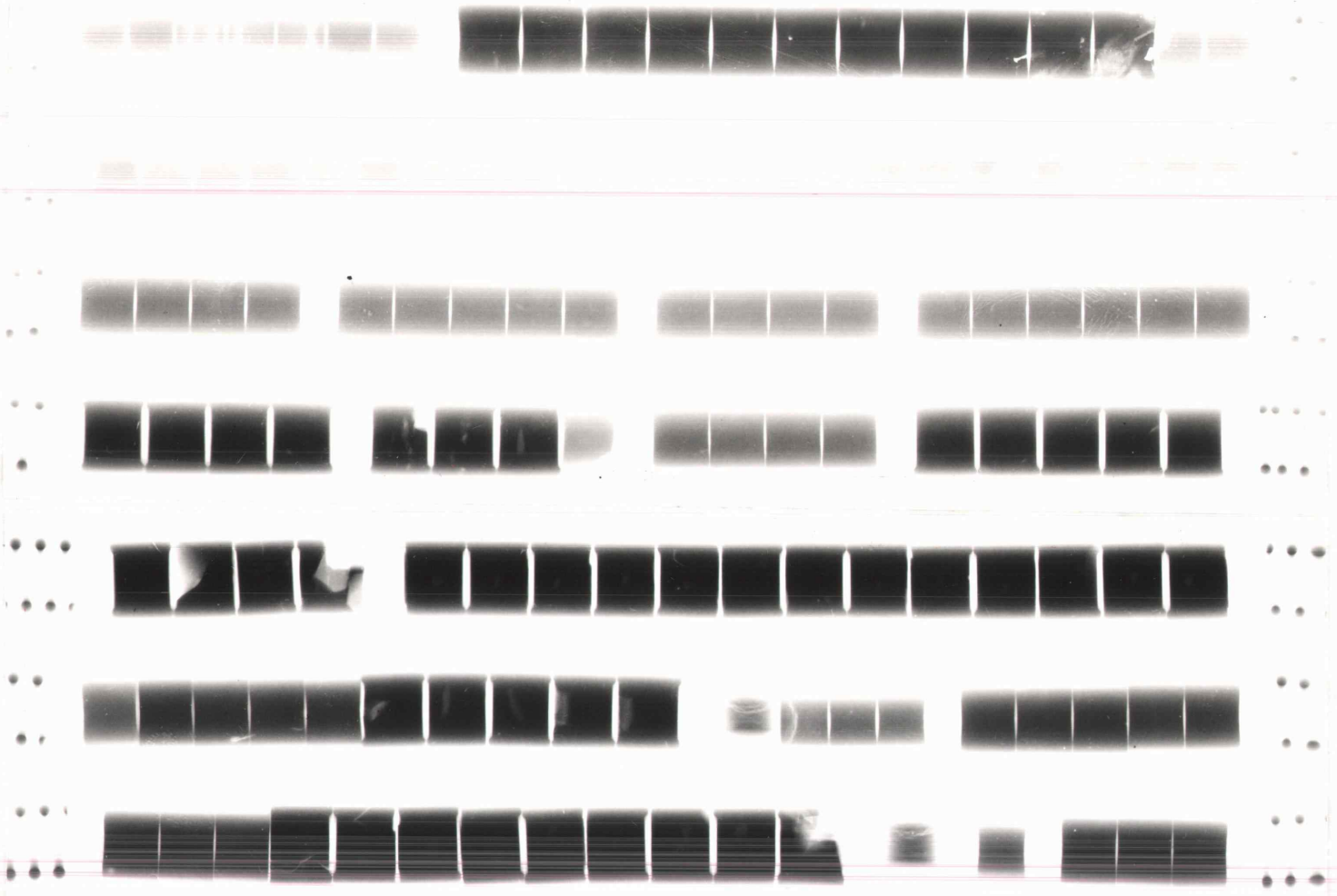

Figure 4.2 Neutron Radiograph of UO_2 Fuel Pins (Taken at 45 degrees)

are not as clearly seen as in the radiographs using a Gd

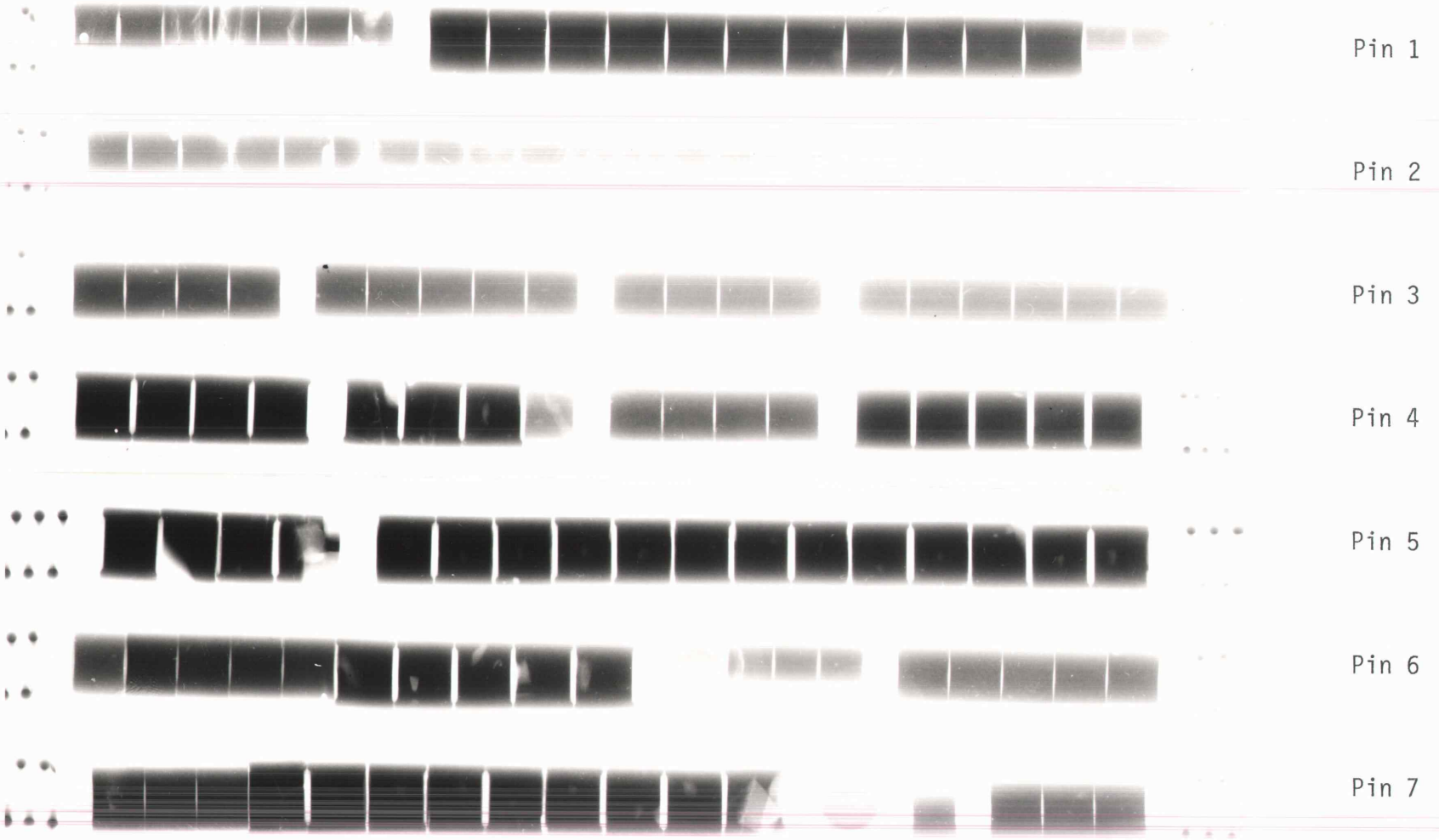

Figure 4.3 Neutron Radiograph of UO_2 Fuel Pins (Taken at 135 degrees)

at the left top of pellet 2 of pin 5, which appears as a triangular shaped defect. However, one cannot tell how deep the defect is from Figure 4.1. The 45 degree picture (Figure 4.2) shows that this pellet is defective into the center of the pellet. The three radiographs of pellet 4 of pin 5 help to determine the shape of a defect in this pellet. The void area looks like a rectangle from the zero degree picture (Figure 4.1), and the other two rotations also show a rectangular shape. Thus, the void is indeed rectangular.

Structural flaws that do not extend all the way through a pellet can be seen in some rotations but not in others. Two structural flaws extend through from the left to the right of pellet 4 of pin 7. These two flaws can be seen very clearly in the 45 degree rotation. However, only one flaw can be seen at the zero rotation, and none of them can be seen in the 135 degree rotation. This means that these two flaws are not very deep. Thus, it is necessary to take pictures with different rotations in order to avoid making an incorrect conclusion.

Some sections of the special fuel pins were also radiographed with ZnS-LiF scintillators. The results obtained with the ZnS-LiF scintillators are presented in Figure 4.4. This figure shows sections of pins 6 and 7. While these radiographs show some defects. These defects are not as clearly seen as in the radiographs using a Gd

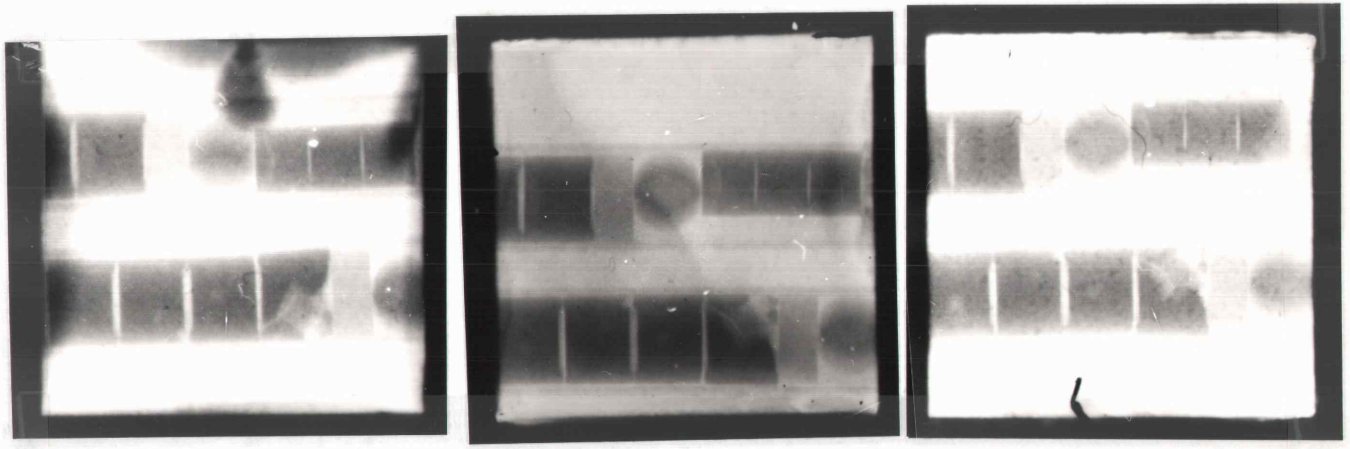

#32 #33 #34

Figure 4.4 Neutron Radiograph of UO_2 Fuel Pins Using ZnS-LiF Scintillators
(Taken at 10 kW, flux: 3.5 X 10^7 n/cm^2-sec-MW, 16 minutes exposure)

foil as the converter screen. Since the art of making scintillators is still being developed, the results of three of the many scintillators made at the OSU are shown. While the resolution of the scintillators is significantly lower than that of the Gd foil, their speed is much greater. Thus, the exposure time can be reduced by a factor of 25. This permits neutron radiography with low flux sources such as ^{252}Cf.

4.2.2 Indium Transfer Thermal Neutron Radiography of Special UO_2 Fuel Pins

Special UO_2 fuel pin 7 was radiographed in the OSTR beam port #1 with indium in a metal cassette for 30 minutes at 1 MW. During the exposure, fuel pin 7 was held in a vertical position and subjected to an integrated thermal flux of about 5.4×10^9 n/cm ^{2}. After the exposure, the indium foil cassette was taken out from beam port # 1. Five minutes later a T-5 X-ray film was put in front of the indium and left overnight while the indium decayed. Film processing was performed as recommended by the manufacturer.

In the transfer method, the activity produced in the transfer screen is directly proportional to the number of neutrons passing through the fuel. Consequently, the activity produced in a neutron radiographic transfer detection screen will be directly related to the attenuation of the fuel pin at each point in the image.

Figure 4.5 shows a positive print of fuel pin 7, which was taken at the zero degree direction. Most of the same defects can be seen that were observed in Figures 4.1, 4.2, and 4.3. Cracks can be seen very easily in pellet 4 of this pin. Pellet 12 was cracked and smashed. The images of cracks and smashed pieces can be seen very clearly.

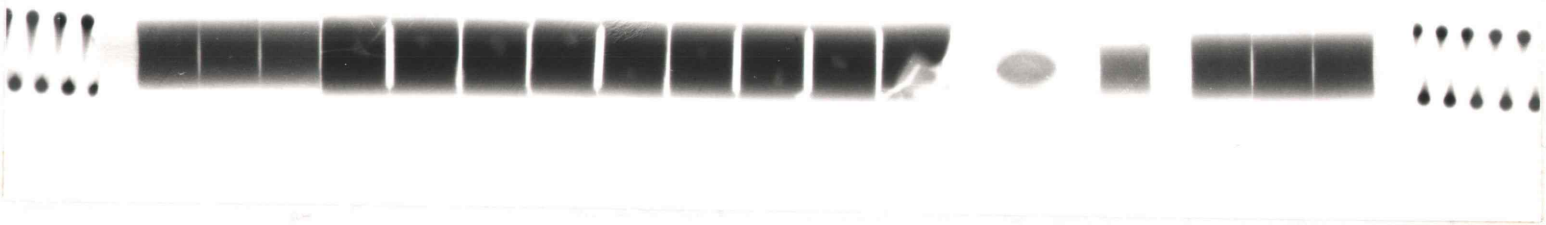

Figure 4.5 Indium Thermal Transfer Radiograph of UO_2 Fuel Pin 7

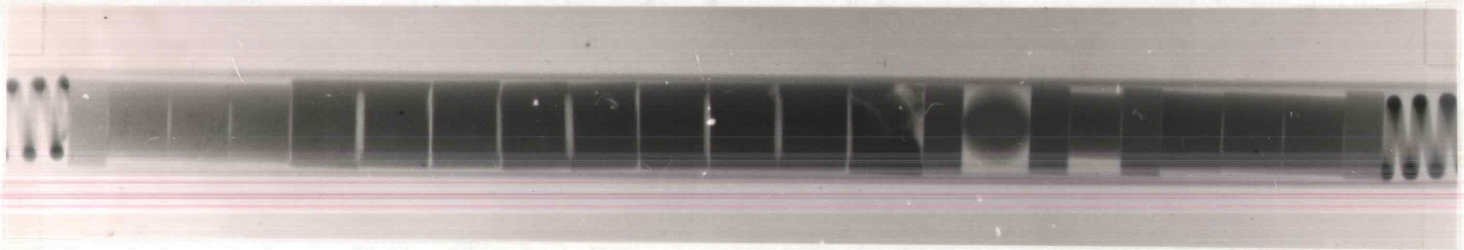

Figure 4.6 Indium Epithermal Radiograph of UO_2 Fuel Pin 7

While this method does not have as high a resolution as the Gd foil, it does allow radiographing highly radioactive objects such as spent fuel.

4.2.3 Epithermal Neutron Radiography of Special UO_2 Fuel Pins

Epithermal neutron radiography is a way of radiographing objects containing a light element material, such as hydrogen. In anticipation of applying this technique to the TRIGA fuel elements, radiographs of the special UO_2 fuel pins were taken. The procedure for epithermal neutron radiography is the same as that for the thermal neutron transfer method, except that a cadmium sheet is placed in front of the object and another one placed in back it. This prevents any thermal neutrons in the beam from reaching the indium foil.

The effect of this technique is to make light element scattering appear as an absorption in the object. If a neutron scatters off a light element, its energy is reduced and it is absorbed in the Cd before reaching the indium detector.

Figure 4.6 shows the positive print of fuel pin 7. The indium cassette was exposed with fuel pin 7 for one hour. Six minutes after exposure a T-5 X-ray film was put in front of the indium in the metal cassette and exposed overnight. Again film processing was performed as recommended by the manufacturer. Some details which can be seen in Figure 4.1, cannot be seen in Figure 4.6. However, most structures and defects can still be seen very clearly

in this picture. These include the zirconium cladding, springs, gap between the cladding and fuel pellets, gap between pellets, the smashed pieces and cracks. Also, a very uniform background was obtained using this method. This means that in this method no radiation other than epithermal neutrons contributed to the image on the T-5 X-ray film exposure. Thus, this method can be applied to radioactive objects.

4.3 Gamma Radiography of Special UO_2 Fuel Pins

The procedure and facility for gamma radiography of fuel pins is the same as that for direct neutron radiography except that no gadolinium converter screen is used.

All seven of the special UO_2 fuel pins were radiographed together using AA X-ray film in a metal cassette. An exposure time of 90 seconds was required for this technique.

Figure 4.7 shows a positive print of the radiograph of all seven fuel pins. The cracks, laminations, structural flaws, and defects of these fuel pins can be seen in this picture. However, they are not as clear as in Figure 4.1.

By comparing Figures 4.1 and 4.7, the following conclusions can be drawn. Although defects can be seen from gamma radiographs, it is easy to see that the neutron radiographs show a greater contrast between areas of different attenuation than do the gamma radiographs. The cracks of pellet 4 in pin 7 can be seen very clearly in Figure 4.1. These cracks can be seen by gamma radiography (Figure 4.7), but not as clearly as in Figure 4.1. For pellet 12 of pin 7, the image of the cracks is superposed on the image of the bigger defect. These two images can be very clearly discriminated by neutron radiography, but not by gamma radiography. In spite of this, gamma radiography is a powerful tool to detect defects in fuel.

Figure 4.7 Gamma Radiograph of UO_2 Fuel Pins

4.4 Summary

The radiography of the special UO_2 fuel elements produced excellent results. The best results were obtained by direct neutron radiography using a gadolinium converter screen.

The main advantages of this direct method over the others are as follows:

1) Speed

Direct neutron radiography using AA X-ray film and a gadolinium foil is three times faster than gamma radiography using the same X-ray film, about 20 times faster than the indium transfer foil method, and 60 to 100 times faster than the epithermal indium foil method.

2) Contrast

The best contrast is obtained by the direct neutron radiography method.

3) Resolution

A gadolinium foil provides optimum radiographic resolution. The excellent resolution qualities of gadolinium foil is to be due to a combination of very high neutron cross section, a fact which permits the use of very thin screens with reasonable exposure times, and the fact that gadolinium emits some soft, easily absorbed radiation (through an internal conversion electron of about 70 keV) upon neutron bombardment.

Based on all of the radiographs presented here, it is easy to see that the direct neutron radiographs using a vapor-deposited gadolinium converter screen in a vacuum cassette provide the best overall detail visibility.

V. NEUTRON AND GAMMA RADIOGRAPHY OF OSTR FUEL ELEMENTS

5. 1 NEUTRON RADIOGRAPHY OF OSTR FUEL ELEMENTS

Based on the experience from the neutron radiography of the special UO_2 fuel elements, the direct neutron radiography method was the first one employed for the OSTR fuel elements. In this study, a Gd foil with either AA or DR-5 X-ray film was used with a metal pressurized cassette or vapor-deposited vacuum cassette.

All of the samples radiographed for this study were either standard or FLIP fuel elements. Some of them had been previously irradiated in the OSTR; others had never been used. The irradiated samples selected for radiography had cooled (in a radioactive sense) sufficiently to handle without remote equipment. Some of these elements had exceeded the dimensional limits in the fuel specifications. For example, standard TRIGA fuel element #4651 has experienced 36 MW-hr of burnup and 1040 pulses. It was selected because it exceeds the bow limit of 0.062 inches and the elongation limit of 0.10 inches. This element had an original length of 24.097 inches and a bow of 0.009 inches, which was within the limits. Another element selected, because of its high exposure in the core, was standard element # 4749. It had an original length of 24.11 inches and a bow of 0.012 inches. This element has

experienced 2015 MW-hr of burnup.

Two elements that had never been irradiated were selected at random from samples of both standard and FLIP elements. The selected elements were standard element #4749 and FLIP element #8402. Standard element #4749 contains 38 grams of ^{235}U and 192 grams of total uranium. Its length is 24.106 inches with a bow of 0.003 inches. FLIP element #8402 contains 134.64 grams of ^{235}U and 192.41 grams of total uranium and has a length of 24.175 inches.

For radiography, these elements were removed from their storage pit with a crane and then placed in beam port #1. Since the radiographs are only 10 inches by 8 inches, three radiographs were required to cover the complete length of a TRIGA fuel element, typically 28.5 inches.

The fuel section of a TRIGA FLIP fuel element consists of three slugs each 5 inches in length. Since the fuel element is a cylinder, the image density of the element is not uniform. Thus, the image of the edge of the fuel looks brighter than that of the center of the fuel due to the non-uniform projection of the cylindrical fuel. Since the atomic density of the zirconium rod is smaller than that of the uranium, the image of the zirconium rod looks brighter than that of the fuel region.

Figure 5.1 shows a positive print of a thermal neutron radiograph of standard fuel element #4749. This radiograph was taken by the direct exposure method using a Gd foil

Figure 5.1 Neutron Radiograph of Standard TRIGA Fuel Element #4749

with DR-5 X-ray film in a plastic pressurized cassette. The film processing was performed as recommended by the manufacturer. The exposure time was 1.5 minutes at 1 MW. Neutron fluence was 2.7×10^9 n/cm^2 and the film density was 1.45. A crack in this fuel element can be seen in this picture, although it is hard to detect.

In order to improve the radiography results, many different variations of technique were tried with thermal neutron radiography. This included changing the type of the film, such as using AA, DR-5, T-5, and No-Screen medical X-ray films; varying the exposure time, from underexposure to overexposure; and selecting different kinds of fuel elements, such as standard OSTR fuel elements #4749 and #4651 and FLIP fuel element #8402. But all the radiographs failed to give satisfactory results due to the neutron scattering problem in the OSTR fuels.

Next, the epithermal indium foil transfer method was employed. This method provided some improvement over the thermal neutron radiographs. Figure 5.2 is a positive print of a radiograph of FLIP fuel element #8402. This element was exposed in beam port #1 for 3 hours. Four minutes later a T-5 film was placed next to the indium foil and exposed overnight. This picture shows better contrast between the fuel slugs, the gaps, and the cladding than does a thermal neutron radiograph. Also the zirconium rod, as well as a displaced part of the zirconium rod, can

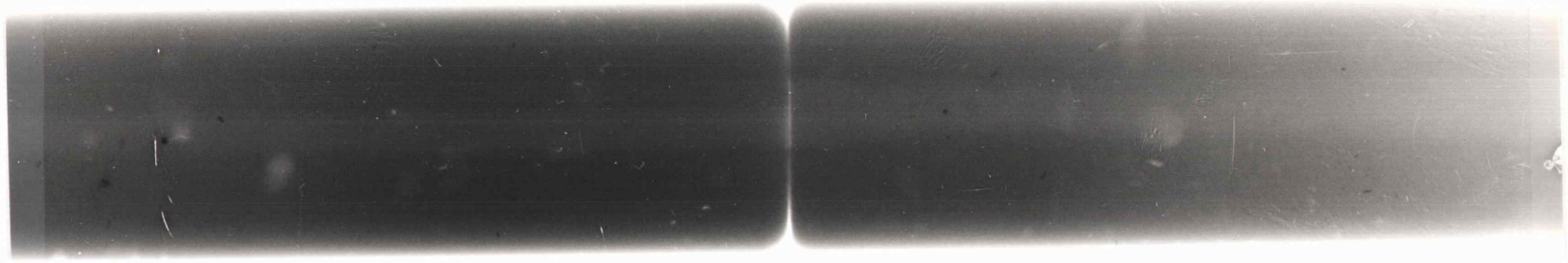

Figure 5.2 Epithermal Neutron Radiograph of FLIP Fuel Element #8402

be seen clearly in the picture. Many different sizes of voids can also be clearly seen in the fuel imaging. Most of them appear to be around the zirconium rod.

Nevertheless, both of these neutron radiography methods suffer from the same basic problem: too much neutron scattering in the object (the fuel element) by hydrogen. For this reason, neutron radiography was abandoned as a means to show the internal structure of TRIGA fuel.

5. 2 Gamma Radiography of OSTR Fuel Elemnts

To some extent, the scattering problem in thick hydrogeneous materials can be lessened by making use of epithermal neutrons and/or employing a neutron absorbing grid to reduce the influence of scattered neutrons. An anti-scatter grid can be used to eliminate the scattered neutrons with angles larger than an acceptable range which depends on the L/D ratio of the grid, where L and D are the length and diameter of the grid respectively. Thus, neutrons with incorrect angles are absorbed. In this way the anti-scatter grid looks like an absorber of larger angle scattered neutrons. This reduces the fogging in the image by the scattered neutrons. However, for large diameter fuel elements, such as TRIGA fuel, a grid will not work. For OSTR fuel, the number density of the hydrogen in the fuel is about 0.061 atoms/barn-cm, which is comparable to 0.0692 atoms/barn-cm for hydrogen in ordinary water. Thus, fuel element looks like a thick cylindrical rod of water to neutrons. Too much hydrogen causes very serious scattering problems in neutron radiography, fogging the image and making it useless.

Fortunately, the scattering problem of hydrogenous materials doesn't occur in gamma radiography because the hydrogen is radiolucent for gamma rays. The ability of gamma radiography for inspecting an object results from the

various densities of materials in the object. The greater the density of the material, the less transmission, and vice versa. The cracks, inclusions, foreign materials, and defects hidden in the object are of lower density compared to the fuel. Thus, the gamma radiographic appearance of a fuel element is considerably altered by the presence of foreign materials, defects, etc.

Because of the successful results with gamma radiography of the special UO_2 fuel, a switch to gamma radiography was made for the TRIGA fuel elements. With this method excellent results were obtained. The procedure for gamma radiography of TRIGA fuels was the same as that used for the UO_2 fuel pins. The TRIGA fuel to be radiographed was removed from a storage pit and placed in beam port #1 where it was exposed to gamma rays from the reactor. The X-ray film in the metal or plastic pressurized cassette was adjacent to the fuel element and was exposed for a suitable time (usually 80 seconds). After exposure, a 5 minute cooling time was used to reduce the intense dose of radiation from the fuel. Most of the films used in this part of the study were AA X-ray films with the processing procedure as recommended by the manufacturer. For the gamma radiographs, AA X-ray film provided sufficient resolution, as seen in the figures presented here, and is about ten times faster than DR-5 film. All of the pictures presented here are positive

prints.

Figure 5.3 shows a gamma radiograph of the top end of standard TRIGA fuel element #4651. This radiograph was taken by using a metal pressurized cassette with AA X-ray film. The exposure was 80 seconds at 1 MW. This produced a film density of 2.72. It shows the gap between the graphite and cladding as well as a crack 6 1/4 inches from the top end of the fuel section. Four voids can be seen in the fuel section, although not very clearly. Three of them are near the middle of the fuel.

Standard fuel elment #4749 was also gamma radiographed using a metal cassette with AA X-ray films. Again the exposure time was 80 seconds at 1 MW. Few defects, as shown in Figure 5.4, can be seen in this picture. The only defect that was observed is a big crack in the middle part of the fuel section.

In order to study FLIP fuel element #8402 thoroughly a set of pictures with different rotations were taken using gamma radiography. Three radiographs were taken at each rotation so that the whole fuel element could be seen. The reference angle (zero degree direction) is designated such that the serial number of the element is facing the vertical direction.

The zirconium rod in element #8402 looks perfect in Figure 5.5, which was taken at the zero direction. However, a displacement of the rod can be seen in Figure 5.6

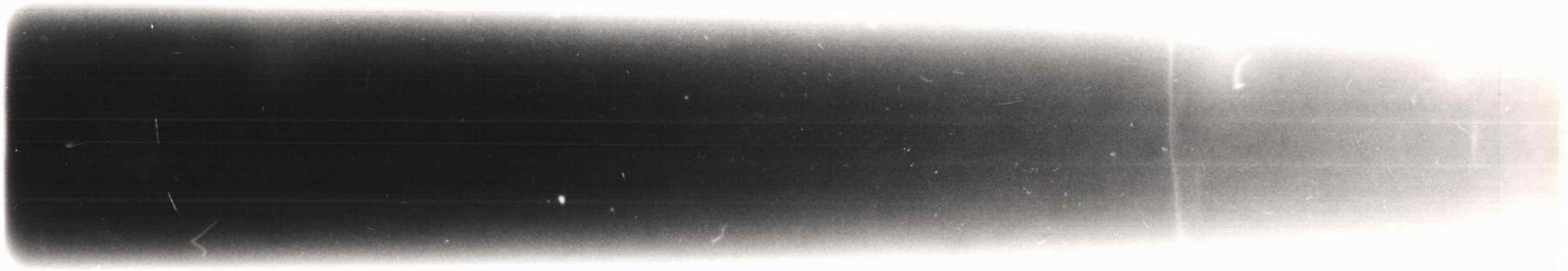

Figure 5.3 Gamma Radiograph of TRIGA Fuel Element #4651

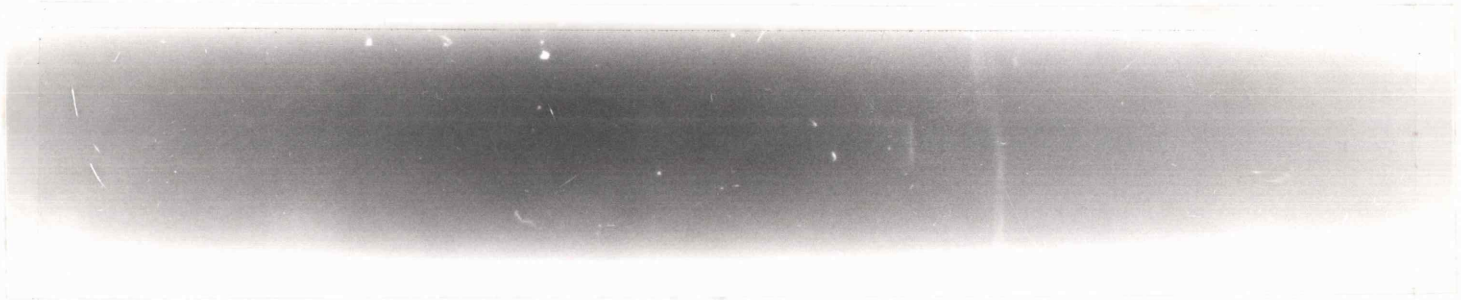

Figure 5.4 Gamma Radiograph of Standard TRIGA Fuel Element #4749

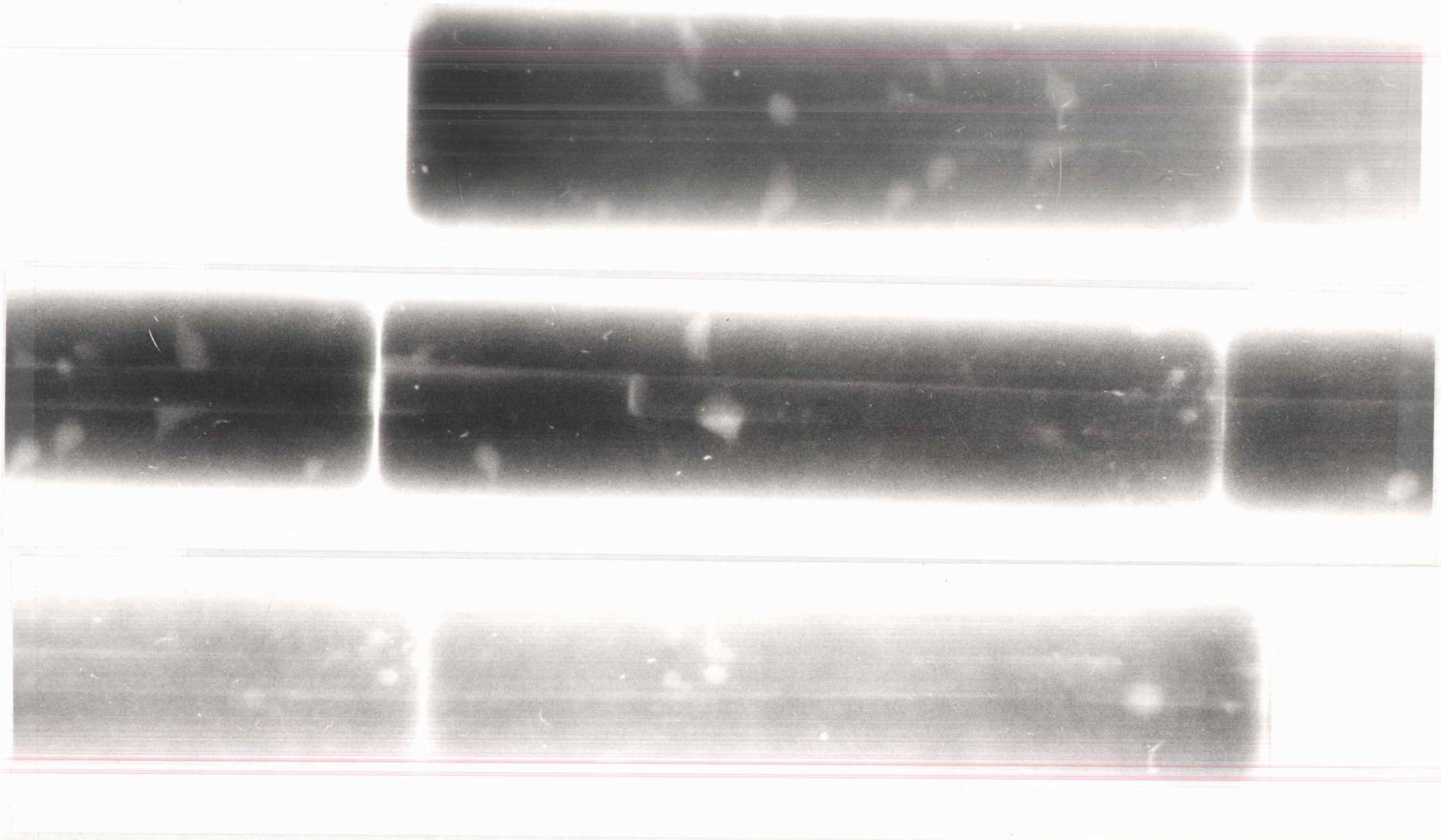

Figure 5.5 Gamma Radiograph of FLIP Fuel Element #8402 (Taken at 0 degree)

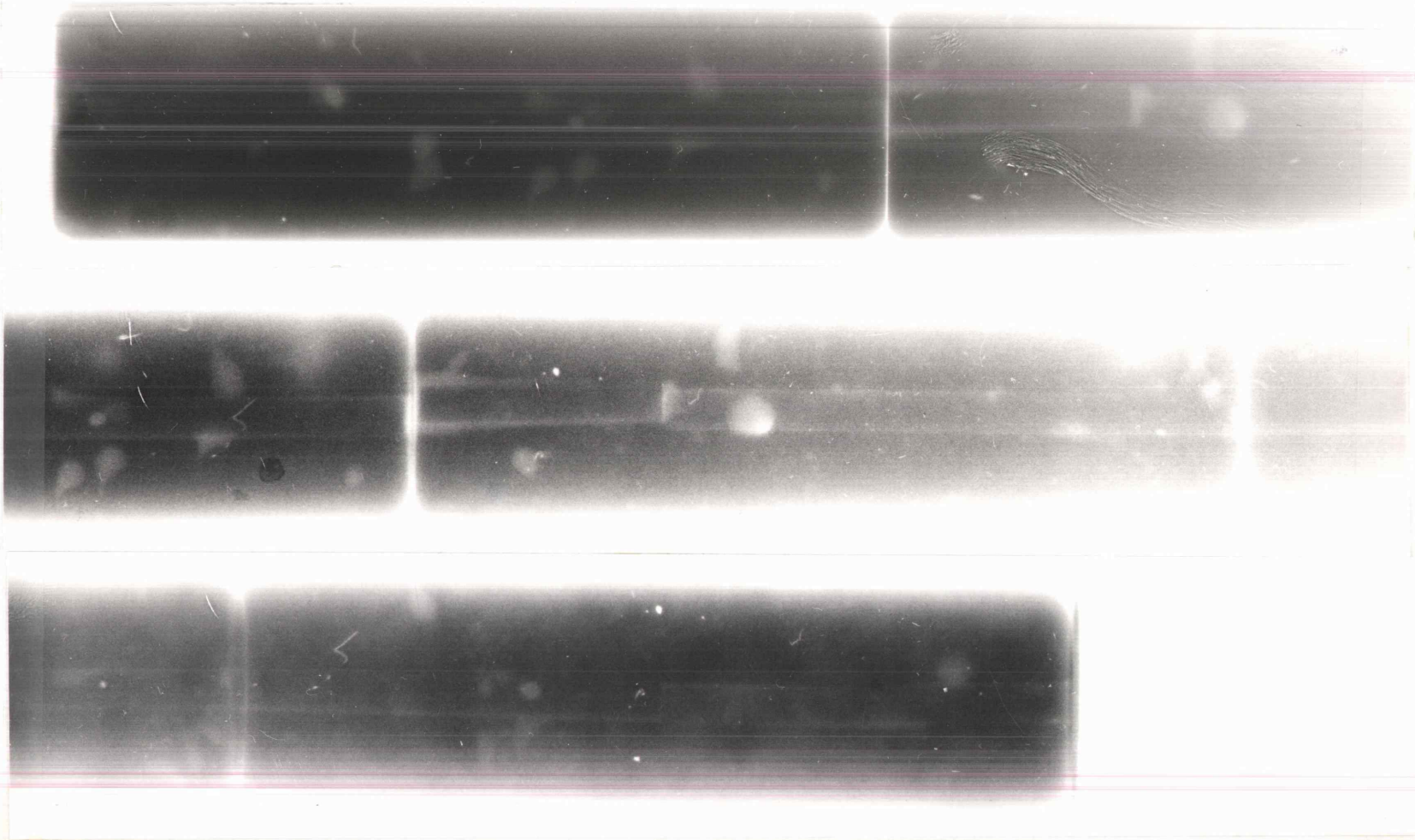

Figure 5.6 Gamma Radiograph of FLIP Fuel Element #8402 (Taken at 25 degrees)

which was taken at 25 degrees. When the rotation was changed continuously from 0 to 90 degrees, a larger and larger displacement of the zirconium rod was observed. Figure 5.7 shows radiographs taken at 70 and 80 degrees rotations. These radiographs, when viewed with a stereopticon, provide a three-dimensional image of the fuel element. Such an image is very helpful in determining the actual internal position of an observed defect. Figure 5.8 shows radiographs taken at 90 and 100 degrees. This stereo pair shows the largest displacement of the center rod. As the rotation is changed from 90 to 180 degrees the displacement of the rod becomes smaller. This is expected as the displacement in the 180 degree rotation should be the same as that in the 0 degree rotation. Figure 5.9 shows a stereo pair taken at 135 and 145 degrees rotations. Another displcement of the center rod is observed at the gap between the middle and top slugs. This displacement can be seen very clearly in Figure 5.10 which was taken at the 120 degree rotation. Many defects and voids are shown in these pictures with nearly half of them occurring near the zirconium rod. The biggest void is about 1/32 of an inch square.

The whole fuel section of the instrumented FLIP fuel element #8486 was gamma radiographed, as shown in Figure 5.11. This fuel element was radiographed with an AA X-ray film in the metal cassette for 80 seconds at 1 MW. The

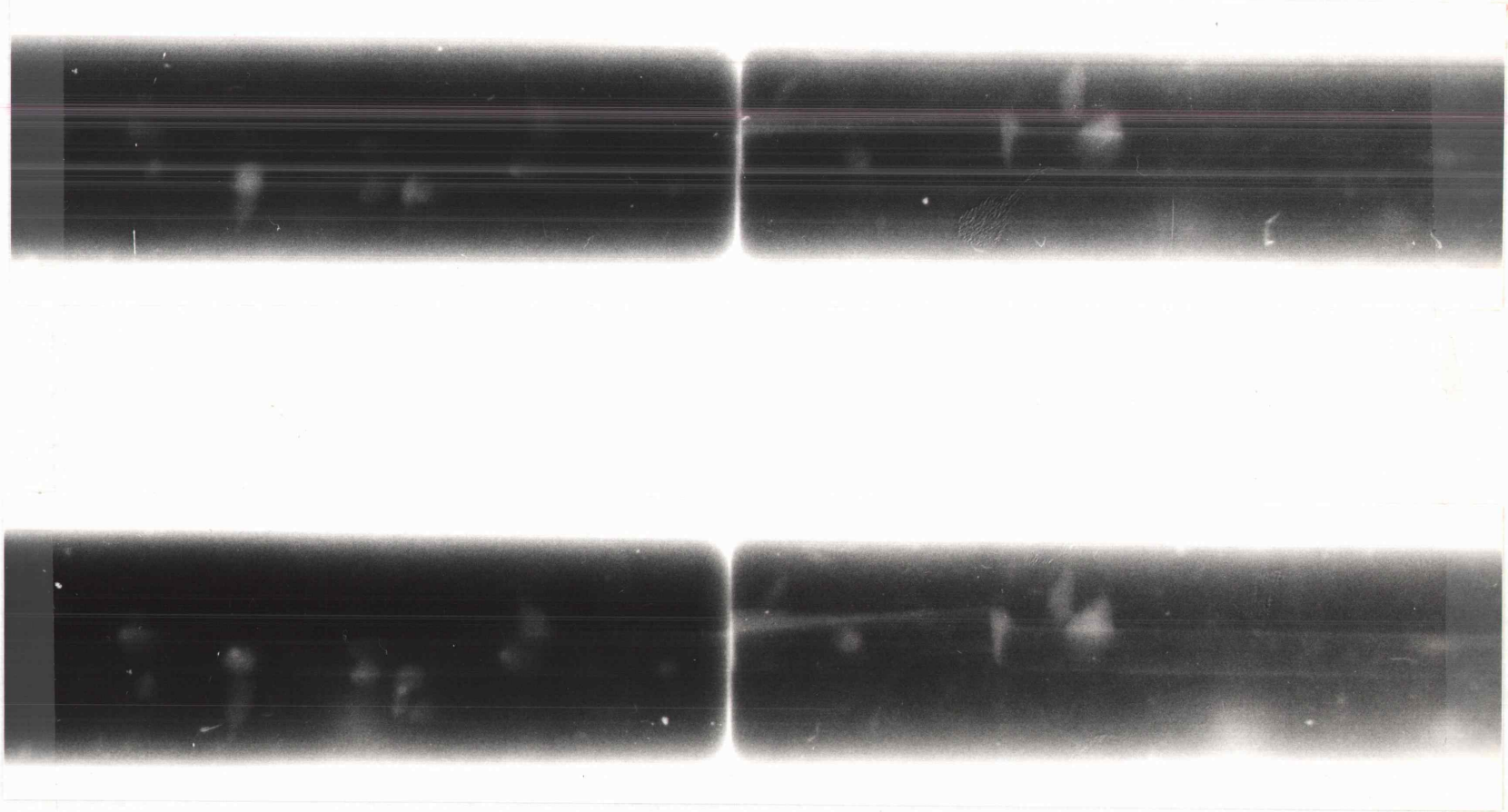

Figure 5.7 Stereo Pairs of Gamma Radiographs of FLIP Fuel Element #8402
(Taken at 70, and 80 degrees)

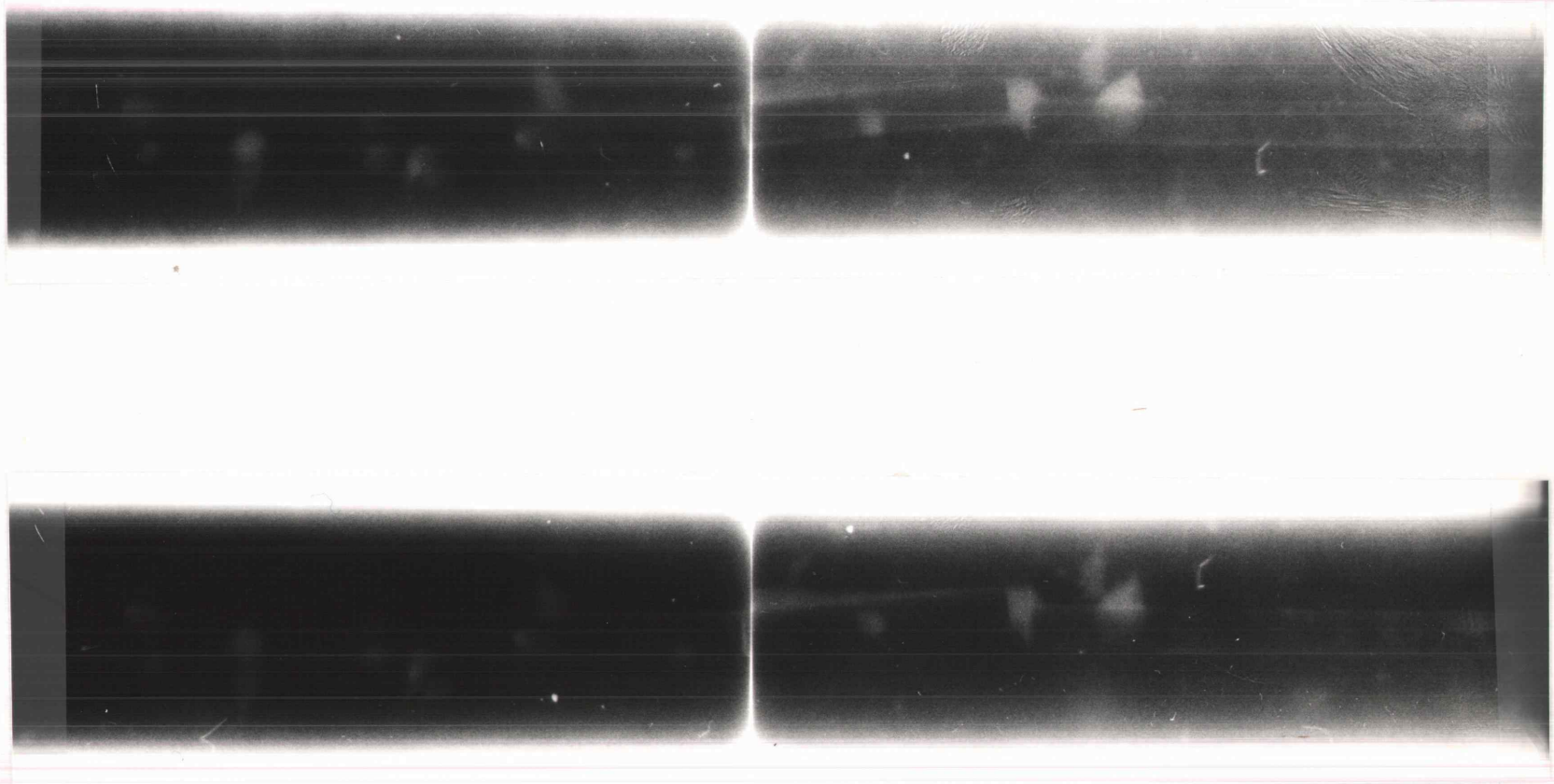

Figure 5.8 Stereo Pairs of Gamma Radiographs of FLIP Fuel Element #8402
(Taken at 90, and 100 degrees)

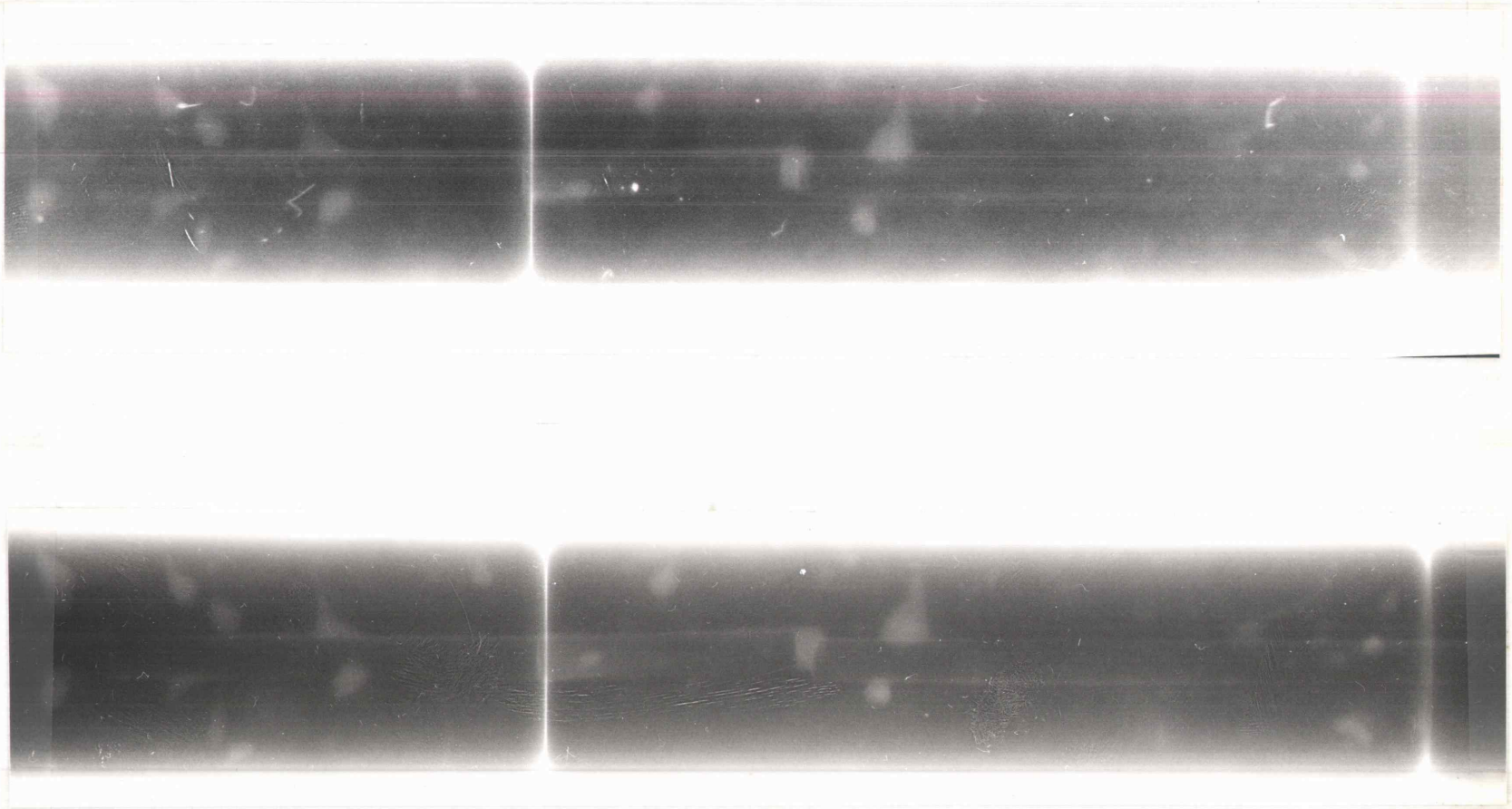

Figure 5.9 Stereo Pairs of Gamma Radiographs of FLIP Fuel Element #8402
(Taken at 135, and 145 degrees)

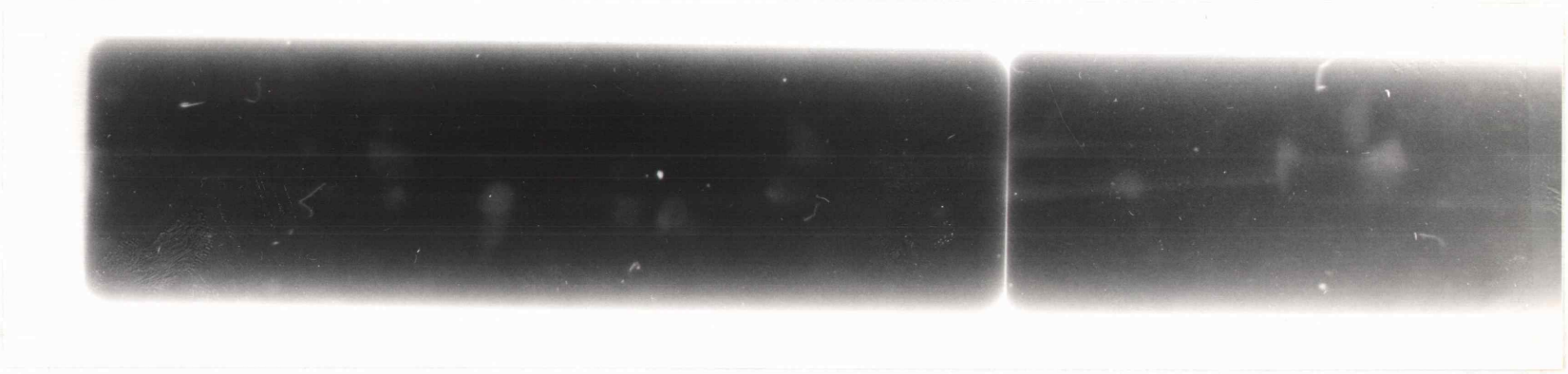

Figure 5.10 Gamma Radiograph of FLIP Fuel Element #8402 (Taken at 120 degrees)

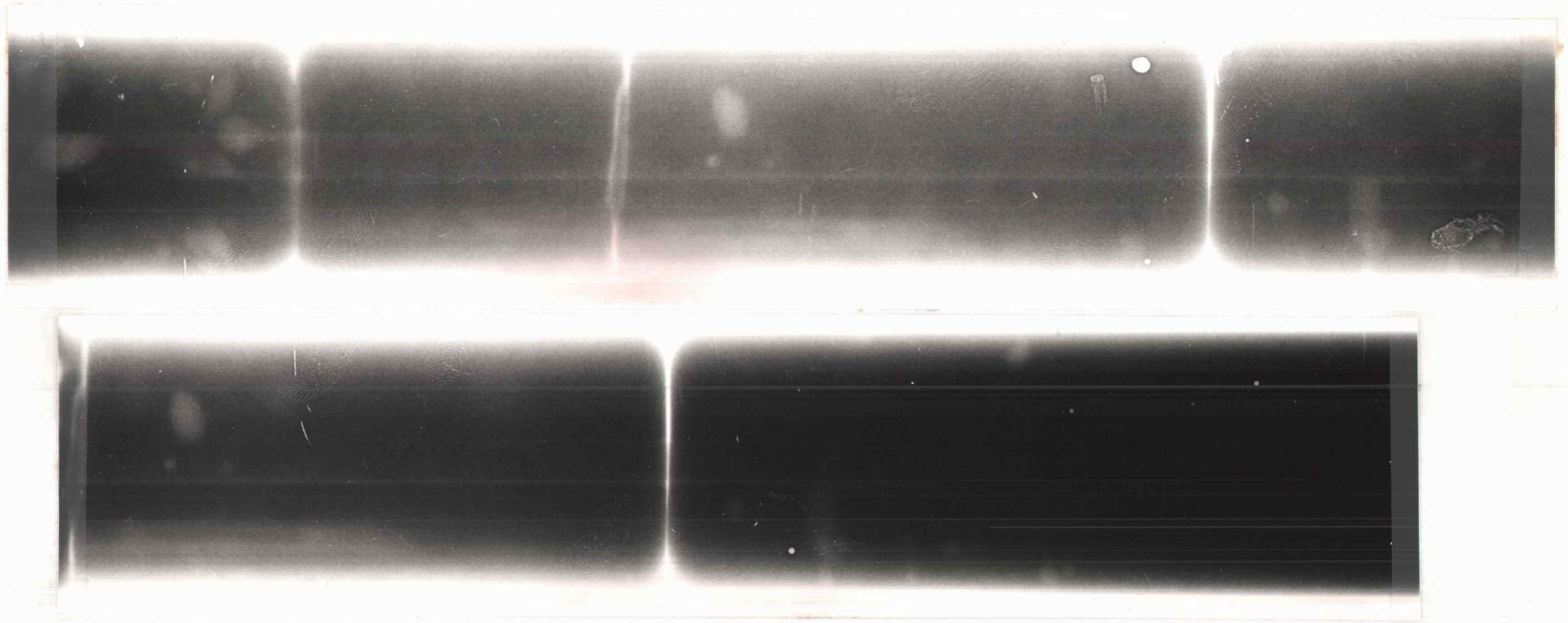

Figure 5.11 Gamma Radiograph of FLIP Instrumented Fuel Element #8486
(Taken at 0 degree)

three pictures in this figure show excellent overall detail for the cladding, gap between slugs, gap between slug and graphite, gaps among the slugs and cladding, and the zirconium rods. Two parallel cracks about 3/4 inches long can be seen near the center of the fuel section. These meet and are combined into one big crack about 1/4 in. away from the cladding. This crack extends across the whole fuel section. Many different sizes of voids can be seen randomly distributed in the fuel section, especially in the top slug. As previously discussed, the instrumented fuel elements contain three thermocouples. In the drawings these thermocouples are shown as slanting across the fuel from the outside toward the centerline. The gamma radiograph (Figure 5.11) shows these thermocouples to be parallel to the axis of the fuel. By taking pictures at different rotations, it was determined that the thermocouples are actually halfway between the clad and the centerline. The thermocouple leadout wires also can be seen in these pictures.

Another instrumented fuel element #7328 was also gamma radiographed. The element is a standard fuel element. Three of these pictures, each with a different rotation, are shown in Figure 5.12. The rotations were 0, 120, and 240 degrees. Four big but not very deep voids are observed in the fuel section of this element. No displacement of the zirconium rod appears in any rotation. Again the

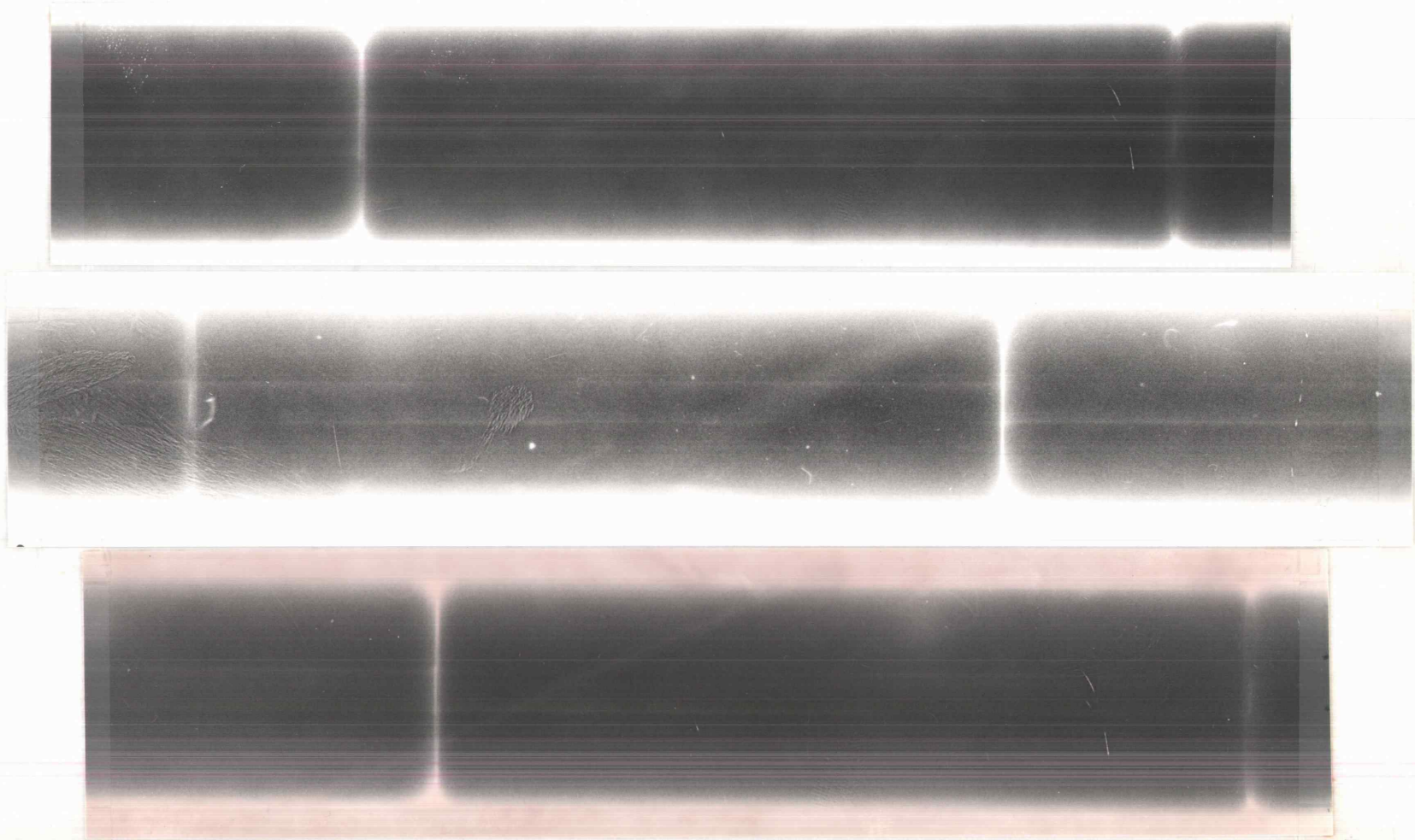

Figure 5.12 Gamma Radiograph of Standard Instrumented Element #7328
(Taken at 0, 120, and 240 degrees, from top to bottom)

thermocouples are seen to be parallel to the axis of the fuel element and not slanted as shown in the drawings. The thermocouple leadout wires can be seen in the zero degree rotation.

Fueled-follower-type control rod element #8945 was selected for gamma radiography as a sample of this type of element. Figure 5.13 was taken at the zero degree rotation. This picture is a positive print of the fuel section of the control rod. The fuel slugs and gap between the slugs can be seen very clearly in this picture. The zirconium rod in the center of the fuel section looks perfect. However, a small displacement of the zirconium rod can be seen in Figure 5.14 which was taken at the 90 degree rotation. The cladding of the control rod can also be seen very clearly in both figures. The radiographs of the control rod do not show any defects, cracks, voids or significant displacements.

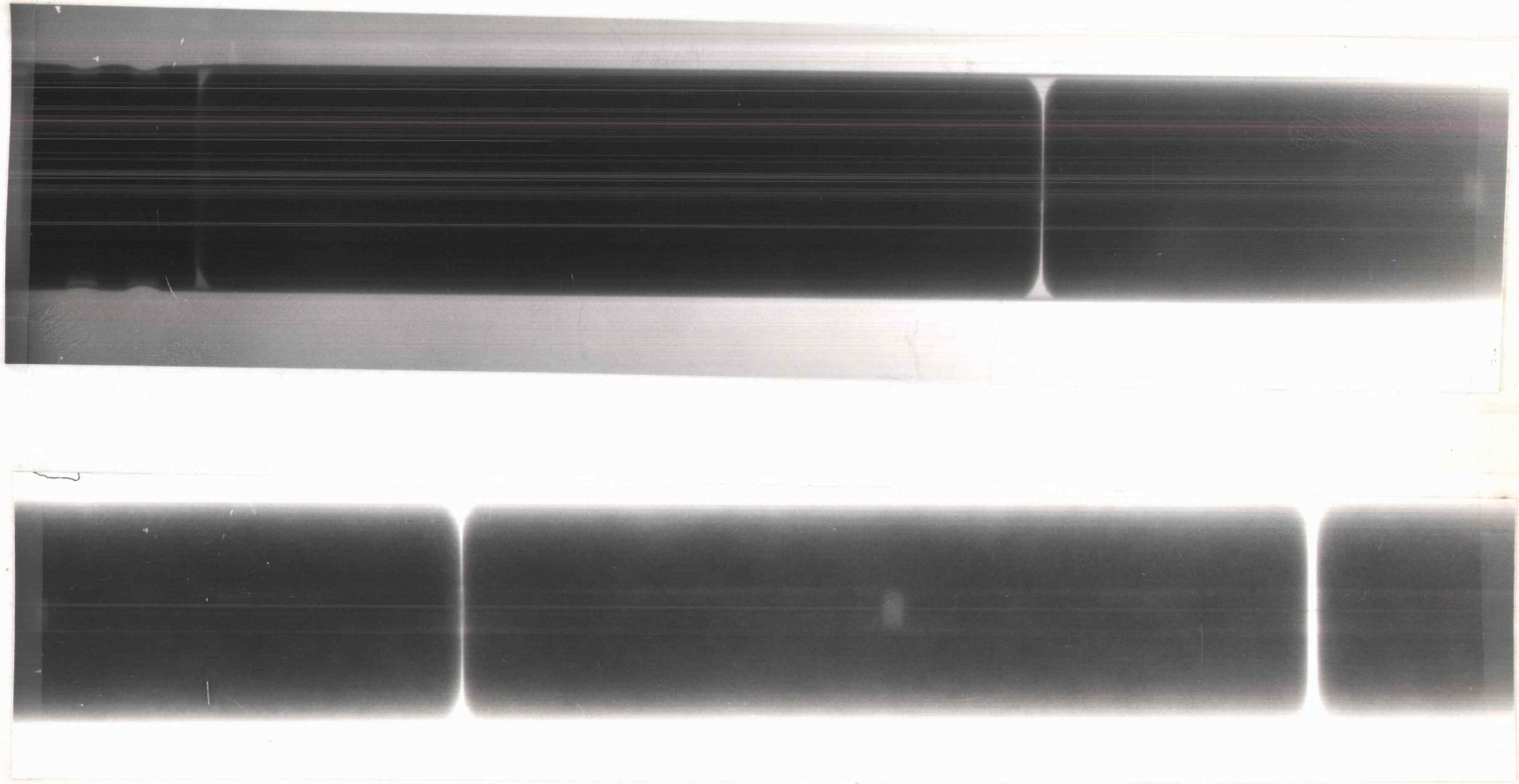

Figure 5.13 Gamma Radiograph of Fueled-follower-type Control Rod #8945
(Follower section)

Figure 5.14 Gamma Radiograph of Fueled-follower-type Control Rod #8945
(follower section, taken at 90 degrees)

VI. CONCLUSIONS

The main purpose of this work was to develop a method whereby the TRIGA fuel elements (including the regular fuel, instrumented fuel, and the control rods) could be radiographed. Such a method was developed but it turned out to be gamma radiography, not neutron radiography, that was the better method.

Neutron radiography is a very useful method for inspecting nuclear fuel elements which do not contain a moderator (such as hydrogen in the TRIGA fuel). Many papers related this area have been published in the last two decades. Radioactive fuel elements have also been neutron radiographed and satisfactory results have been obtained.

In this study, the special UO_2 fuel pins were radiographed by means of neutron, X-, and gamma radiography. The results showed that the direct neutron radiography was superior to the others.

The first method employed for inspecting the internal structure of TRIGA fuel was direct neutron radiography. The results showed that the cladding and gaps could be seen, but not the internal structure of the fuel itself.

In order to improve the situation many attempts were made, such as changing the type of the film, varying the exposure times, and selecting different types of TRIGA

fuel. They all failed to give satisfactory results.

The indium foil transfer method, both thermal and epithermal, was another attempt. Although the results were improved to some extent, the imaging of the fuel section still was far from satisfactory due to the scattering problem caused by hydrogen.

Because of the relatively large diameter of the TRIGA fuel elements (compared to the UO_2 rods), a neutron may scatter many times before exiting the element. These scattered neutrons destroy the image of the internal structure of the element.

Since hydrogen scattering problems do not exsit for gamma radiography, this method was employed for inspecting TRIGA fuel in this study. Before trying this method for TRIGA fuel, the UO_2 fuel was radiographed in order to see the difference between neutron and gamma radiography where both can be used. Because of the excellent results of the UO gamma radiography, gamma radiographs of the TRIGA fuel elements were taken. These again showed excellent results.

Examples of the results obtained were the fact that many different sizes of voids, cracks, defects and the displacement of the zirconium rod exist in FLIP fuel element #8402. In addition to many different sizes of voids, two big cracks were also found in instrumented fuel element #8486. Voids, cracks, and defects could be seen in standard fuel elements #4749 and #4651, but they were not

very serious. No voids, cracks, or defects were observed in control rod element #8945. Only a small displacement of the zirconium rod of this control rod was observed.

Although the displacement in #8402 will change the thermal flux distribution of this element, it is unlikely to affect the peak flux significantly.

One question remained. Could these fuel elements still be used in the reactor? To answer this question gamma radiographs of the elements were sent to the manufacturer, who reviewed the radiographs and stated that the elements were acceptable for use (53).

A comparison of the neutron and gamma radiography for the UO_2 fuel elements shows that the gamma radiographs will show most of the defects visible in the neutron radiographs. However, for TRIGA fuel elements only gamma radiography can show the internal structure.

VII. REFERENCES

1. H. Kallman, E. Kuhn, Die Naturwissenschaften, Vol. 25, 1937, p.231.
2. H. Thewils, "Neutron Radiography," British Journal of Applied Physics, Vol. 7, 1956, p. 345.
3. H. Berger, Neutron Radiography, Elsevier, N.Y., 1965.
4. J.P. Barton, "Neutron Radiography-An Overview," Practical Applications of Neutron Radiography and Gaging, ASTM STP 586, American Society for Testing and Materials, 1976, p. 5.
5. M.R. Hawkesworth, J. Walker, "Radiography with Neutrons," Journal of Materials Science, Vol. 4, 1969, p. 817.
6. H. Berger, "The Present State of Neutron Radiography and Its Potential," Materials Evaluation, Vol.30, 1972, No. 3, p. 55.
7. A.R. Spowart, "Neutron Radiography," Journal of Physics E, Vol. 5, 1972, p. 497.
8. M.R. Hawkesworth, Ed.,"Radiography with Neutrons," Conference at the University of Birmingham, September 1973, British Nuclear Energy Society, London, 1975.

9. H. Berger, Ed., Practical Applications of Neutron Radiography and Gaging, ASTM STP 586, American Society for Testing and Materials, 1976.

10. Bloom, W.H., Jr., J.L. Hollenbach and J.A. Morgon, Medical Radiographic Technique, Charles C. Thomas Publishers, 3rd edition, 1965.

11. The Fundamentals of Radiography, Eastman Kodak Company, 1960.

12. A.H. Robinson, C.R. Porter, "Stereoscopic and Stop Action Neutron Radiography of Biological Objects," Biomedical Sciences Instrumentation, Vol. 6, p. 104, 1969.

13. K.G. Galliher, L.W. Hanna, "Neutron Radiography of Apollo Ordnance," Materials Evaluation, Vol. 29, 1971, No. 8, p. 165.

14. J.J Haskins, J.F. Jaklevick, C.D. Wilkinson, "Applications of Neutron Radiography in Fast Reactor Fuel Development," Proceedings of 16th Conference on Remote System Technology, Remote System Division of the American Nuclear Society, Idaho Falls, Idaho, March 1969, p. 218.

15. G. Farny, "Neutron Radiography of Irradiated Fuel Elements Using Celluose Nitrate," Radiography with Neutrons, M.R. Hawkesworth, Ed., Conference at the University of Birmingham, September 1973.

16. K.D. Kok, "Neutron Radiography of Nuclear Fuels at the Battelle Research Reactor," Practical Applications of Neutron Radiography and Gaging, ASTM STP 586, American Society for Testing and Materials, 1976, p. 183.

17. A.M. Ross, "Detecting Cladding Leaks in Irradiated Fuel Elements by Neutron Radiography," Practical Applications of Neutron Radiography and Gaging, ASTM STP 586, American Society for Testing and Materials, 1976, p. 195.

18. C.N. Jackson, Jr., H.G. Powers, C.A. Burgess, "Neutron Radiography of Fuel Pins," Practical Applications of Neutron Radiography and Gaging, ASTM STP 586, American Society for Testing and Materials, 1976, p. 210.

19. W.J. Richards and G.C. McClellan, "Neutron Radiography at the Hot Fuel Examination Facility," Proceedings of 27th Conference on Remote System Technology, 1979.

20. Berger, H., Talboy, J.H., and Tylka, J.P., Nuclear Science and Engineering, Vol. 18, 1964, pp. 236-241.

21. D.J. Hagenmaier, J. Halchak, G. Basl, "Detection of Titanium Hydride by Neutron Radiography," Materials Evaluation, Vol. 27, 1969, No. 9, p. 193.

22. Edenborough, N.B., "Neutron Radiography to Detect Residual Core in Investment Cast Turbine Airfoils," Practical Applications of Neutron Radiography and Gaging, ASTM STP 586, American Society for Testing and Materials, 1976, pp.152-157.

23. J. John, "Californium-Based Neutron Radiography for Corrosion Detection in Aircraft," Practical Applications of Neutron Radiography and Gaging, ASTM STP 586, American Society for Testing and Materials, 1976, pp. 168-180.

24. J.P. Barton, "Some Possibilities Of Neutron Radiography," Physics of Medicine and Biology, Vol. 9, 1964, No. 1, p. 33.

25. H.L. Atkins, "Biological Application of Neutron Radiography," Materials Evaluation, Vol. 23, 1965, No. 9, P. 453.

26. M. Brown, P.B. Parks, "Neutron Radiography In Biological Media: Techniques, Observations and Implications," American Journal of Roentgenology, Radium Therapy, and Nuclear Medicine, Vol. 106, July 1969, p. 472.

27. B.J. Boyne, W.L. Whittemore, "Neutron Radiography of Osseous Tumors," Oral Surgery, Oral Medicine and Oral Pathology, Vol. 31, February 1971, p. 152.

28. J.P. Barton, "Radiography Examination through Steel Using Cold Neutrons," British Journal of Applied Physics, Vol. 16, 1965, p. 1833.

29. M.R. Hawkesworth, J. Walker, "Cold Neutron Beams for Radiography through Steel," Radiography with Neutrons, M.R. Hawkesworth, Ed., Conference at the University of Birmingham, September 1973.

30. J.P. Barton, "Radiography with Resonance Energy Neutrons," Physics of Medicine and Biology, Vol. 10, 1965, p. 209.

31. A.R. Spowart, "The Advantages of Epicadmium Neutron Beams in Neutron Radiography," Non-destructive Testing, February 1968.

32. H.Berger, "Some Experiments In Fast Neutron Radiography," Materials Evaluation, Vol. 27, 1969, No. 12, p. 368.

33. H. Rapp, E. Rachle, D. Ruffner, "Radiography with Fast Neutrons from a Plasma Focus," Materials Evaluation, Vol. 33, 1975, No. 11, p.269.

34. C.B. Shaw, J.L. Cason, "Portable Neutron Radiographic Camera Using Californium-252," Materials Evaluation, Vol. 29, 1971, No. 2, p. 40.

35. D.G. Vasilik, R.L. Murri, G.P. Fisher, "Thermal-Neutron Radiography with a Sealed Tube Neutron Generator and Water Moderator," Nuclear Technology, Vol. 14, 1972, p. 279.

36. J.P. Barton, "Developments in the Use of Californium-252 for Neutron Radiography," Nuclear Technology, Vol. 15, 1972, p. 56.

37. "Californium-252," Progress Report No. 17, USAEC, Aiken, S.C., 1974, pp. 40-41.

38. H. Berger, "Recent Progress in Neutron Imaging," British Journal of Nondestructive Testing, Vol. 10, 1968, No.2, p. 26.

39. K. Valentine, S. Kaplan, B. Perez-Menden, L. Kautman, "A Multimire Proportional Chamber for Imaging Thermal, Epithermal and Fast Neutrons," IEEE Transactions On Nuclear Science, February 1974, p. 178.

40. H. Berger, "Track-Etch Radiography: Alpha, Proton and Neutron," Nuclear Technology, Vol. 19, 1973, p. 188.

41. A.H. Robinson, J.P. Barton, Transactions of the American Nuclear Society, Vol. 1, No. 1, 1972, p. 140.

42. B.L. Blanks, R.A. Morris, "Experiments with Foil-Film Combinations and Collimators for Neutron Radiography," Materials Evaluation, Vol. 24, 1969, No. 2, p. 76.

43. J.P. Barton, "Divergent Beam Collimator for Neutron Radiography," Materials Evaluation, Vol. 25, 1967, p. 45A.

44. A. Choudry, P.K. Bandopadhyay, "Thermal Neutron Focusing By Tapered Rectangular Collimators," Nuclear Instruments and Methods, Vol. 92, 1971, p. 339.

45. T. Wall and R. Gillespie, "Determination of Optimum Foil Exposure Times in Neutron Radiogrpahy Using the Transfer Method," Radiography with Neutrons, M.R. Hawkesworth, Ed., Conference at the University of Birmingham, September 1973.

46. Barton, J.P. and Pervers, J. P., "Underwater Neutron Radiography with Conical Collimators," Brit. J. Nondestructive Testing 79-83. (1966).

47 C.T. Oien, "Feasibility of Neutron Radiographing Reactor Fuel Assemblies," Masters Thesis, Oregon State University, Corvallis, OR., 1976.

48. S.K.L. Wang, "High Speed Motion Neutron Radiography of Two-Phase Flow," Masters Thesis, Oregon State University, Corvallis, OR., 1980.

49. D.A. Tollefson, "Application of High Speed Motion Neutron Radiography Techniques to Liquid Streams Injected into a Pressurized Steel Chamber," Masters Thesis, Oregon State University, Corvallis, OR., 1981.

50. "TRIGA Mark II Reactor General Specifications and Description," General Atomic, GA-2627 (Rev.), March 1964.

51. J.C. Ringle, T.V. Anderson, A.G. Johnson, Safety Analysis Report for the Oregon State University TRIGA Reactor, August 1968.

52. R.H. Bossi, "High Speed Motion Neutron Radiography," Ph.D. Thesis, Oregon State University, Corvallis, OR., 1977.

53. Private communication from General Atomic Company.